FERMI LARGE AREA TELESCOPE STUDY OF COSMIC RAYS AND THE INTERSTELLAR MEDIUM IN NEARBY MOLECULAR CLOUDS

M. ACKERMANN[1], M. AJELLO[2], A. ALLAFORT[2], L. BALDINI[3], J. BALLET[4], G. BARBIELLINI[5,6], D. BASTIERI[7,8], K. BECHTOL[2], R. BELLAZZINI[3], B. BERENJI[2], R. D. BLANDFORD[2], E. D. BLOOM[2], E. BONAMENTE[9,10], A. W. BORGLAND[2], E. BOTTACINI[2], T. J. BRANDT[11,12], J. BREGEON[3], M. BRIGIDA[13,14], P. BRUEL[15], R. BUEHLER[2], G. BUSETTO[7,8], S. BUSON[7,8], G. A. CALIANDRO[16], R. A. CAMERON[2], P. A. CARAVEO[17], J. M. CASANDJIAN[4], C. CECCHI[9,10], E. CHARLES[2], A. CHEKHTMAN[18,63], J. CHIANG[2], S. CIPRINI[10,19], R. CLAUS[2], J. COHEN-TANUGI[20], J. CONRAD[21,22,64], F. D'AMMANDO[9,23,24], A. DE ANGELIS[25], F. DE PALMA[13,14], C. D. DERMER[26], S. W. DIGEL[2], E. DO COUTO E SILVA[2], P. S. DRELL[2], A. DRLICA-WAGNER[2], L. FALLETTI[20], C. FAVUZZI[13,14], S. J. FEGAN[15], E. C. FERRARA[27], W. B. FOCKE[2], Y. FUKAZAWA[28], Y. FUKUI[29], S. FUNK[2], P. FUSCO[13,14], F. GARGANO[14], D. GASPARRINI[19], S. GERMANI[9,10], N. GIGLIETTO[13,14], F. GIORDANO[13,14], M. GIROLETTI[30], T. GLANZMAN[2], G. GODFREY[2], I. A. GRENIER[4,31], M.-H. GRONDIN[32,33], J. E. GROVE[26], S. GUIRIEC[34], D. HADASCH[16], Y. HANABATA[28], A. K. HARDING[27], K. HAYASHI[28], D. HORAN[15], X. HOU[35], R. E. HUGHES[36], R. ITOH[28], M. S. JACKSON[22,37], G. JÓHANNESSON[38], A. S. JOHNSON[2], T. KAMAE[2], H. KATAGIRI[39], J. KATAOKA[40], J. KNÖDLSEDER[11,12], M. KUSS[3], J. LANDE[2], S. LARSSON[21,22,41], S.-H. LEE[42], M. LEMOINE-GOUMARD[43,65], F. LONGO[5,6], F. LOPARCO[13,14], M. N. LOVELLETTE[26], P. LUBRANO[9,10], P. MARTIN[44], M. N. MAZZIOTTA[14], J. E. MCENERY[27,45], J. MEHAULT[20], P. F. MICHELSON[2], W. MITTHUMSIRI[2], T. MIZUNO[28], A. A. MOISEEV[45,46], C. MONTE[13,14], M. E. MONZANI[2], A. MORSELLI[47], I. V. MOSKALENKO[2], S. MURGIA[2], M. NAUMANN-GODO[4], R. NEMMEN[27], S. NISHINO[28], J. P. NORRIS[48], E. NUSS[20], M. OHNO[49], T. OHSUGI[50], A. OKUMURA[2,49], N. OMODEI[2], E. ORLANDO[2], J. F. ORMES[51], M. OZAKI[49], D. PANEQUE[2,52], J. H. PANETTA[2], D. PARENT[18,63], M. PESCE-ROLLINS[3], M. PIERBATTISTA[4], F. PIRON[20], G. PIVATO[8], T. A. PORTER[2], S. RAINÒ[13,14], R. RANDO[7,8], M. RAZZANO[3,53], A. REIMER[2,54], O. REIMER[2,54], C. ROMOLI[8], M. ROTH[55], T. SADA[28], H. F.-W. SADROZINSKI[53], D. A. SANCHEZ[32], C. SBARRA[7], C. SGRÒ[3], E. J. SISKIND[56], G. SPANDRE[3], P. SPINELLI[13,14], A. W. STRONG[44], D. J. SUSON[57], H. TAKAHASHI[50], T. TAKAHASHI[49], T. TANAKA[2], J. G. THAYER[2], J. B. THAYER[2], D. J. THOMPSON[27], L. TIBALDO[7,8], O. TIBOLLA[58], M. TINIVELLA[3], D. F. TORRES[16,59], G. TOSTI[9,10], A. TRAMACERE[2,60,61], E. TROJA[27,66], Y. UCHIYAMA[2], T. UEHARA[28], T. L. USHER[2], J. VANDENBROUCKE[2], V. VASILEIOU[20], G. VIANELLO[2,60], V. VITALE[47,62], A. P. WAITE[2], P. WANG[2], B. L. WINER[36], K. S. WOOD[26], H. YAMAMOTO[29], Z. YANG[21,22], AND S. ZIMMER[21,22]

[1] Deutsches Elektronen Synchrotron DESY, D-15738 Zeuthen, Germany
[2] W. W. Hansen Experimental Physics Laboratory, Kavli Institute for Particle Astrophysics and Cosmology, Department of Physics and SLAC National Accelerator Laboratory, Stanford University, Stanford, CA 94305, USA
[3] Istituto Nazionale di Fisica Nucleare, Sezione di Pisa, I-56127 Pisa, Italy
[4] Laboratoire AIM, CEA-IRFU/CNRS/Université Paris Diderot, Service d'Astrophysique, CEA Saclay, F-91191 Gif sur Yvette, France
[5] Istituto Nazionale di Fisica Nucleare, Sezione di Trieste, I-34127 Trieste, Italy
[6] Dipartimento di Fisica, Università di Trieste, I-34127 Trieste, Italy
[7] Istituto Nazionale di Fisica Nucleare, Sezione di Padova, I-35131 Padova, Italy
[8] Dipartimento di Fisica "G. Galilei," Università di Padova, I-35131 Padova, Italy
[9] Istituto Nazionale di Fisica Nucleare, Sezione di Perugia, I-06123 Perugia, Italy
[10] Dipartimento di Fisica, Università degli Studi di Perugia, I-06123 Perugia, Italy
[11] CNRS, IRAP, F-31028 Toulouse cedex 4, France
[12] GAHEC, Université de Toulouse, UPS-OMP, IRAP, Toulouse, France
[13] Dipartimento di Fisica "M. Merlin" dell'Università e del Politecnico di Bari, I-70126 Bari, Italy
[14] Istituto Nazionale di Fisica Nucleare, Sezione di Bari, I-70126 Bari, Italy
[15] Laboratoire Leprince-Ringuet, École polytechnique, CNRS/IN2P3, Palaiseau, France
[16] Institut de Ciències de l'Espai (IEEE-CSIC), Campus UAB, 08193 Barcelona, Spain
[17] INAF-Istituto di Astrofisica Spaziale e Fisica Cosmica, I-20133 Milano, Italy
[18] Center for Earth Observing and Space Research, College of Science, George Mason University, Fairfax, VA 22030, USA
[19] Agenzia Spaziale Italiana (ASI) Science Data Center, I-00044 Frascati (Roma), Italy
[20] Laboratoire Univers et Particules de Montpellier, Université Montpellier 2, CNRS/IN2P3, Montpellier, France
[21] Department of Physics, Stockholm University, AlbaNova, SE-106 91 Stockholm, Sweden
[22] The Oskar Klein Centre for Cosmoparticle Physics, AlbaNova, SE-106 91 Stockholm, Sweden
[23] IASF Palermo, I-90146 Palermo, Italy
[24] INAF-Istituto di Astrofisica Spaziale e Fisica Cosmica, I-00133 Roma, Italy
[25] Dipartimento di Fisica, Università di Udine and Istituto Nazionale di Fisica Nucleare, Sezione di Trieste, Gruppo Collegato di Udine, I-33100 Udine, Italy
[26] Space Science Division, Naval Research Laboratory, Washington, DC 20375-5352, USA
[27] NASA Goddard Space Flight Center, Greenbelt, MD 20771, USA
[28] Department of Physical Sciences, Hiroshima University, Higashi-Hiroshima, Hiroshima 739-8526, Japan; hayashi@hep01.hepl.hiroshima-u.ac.jp, mizuno@hep01.hepl.hiroshima-u.ac.jp
[29] Department of Physics and Astrophysics, Nagoya University, Chikusa-ku Nagoya 464-8602, Japan
[30] INAF Istituto di Radioastronomia, I-40129 Bologna, Italy
[31] Institut Universitaire de France, F-75005 Paris, France
[32] Max-Planck-Institut für Kernphysik, D-69029 Heidelberg, Germany
[33] Landessternwarte, Universität Heidelberg, Königstuhl, D-69117 Heidelberg, Germany
[34] Center for Space Plasma and Aeronomic Research (CSPAR), University of Alabama in Huntsville, Huntsville, AL 35899, USA
[35] Centre d'Études Nucléaires de Bordeaux Gradignan, IN2P3/CNRS, Université Bordeaux 1, BP120, F-33175 Gradignan Cedex, France
[36] Department of Physics, Center for Cosmology and Astro-Particle Physics, The Ohio State University, Columbus, OH 43210, USA
[37] Department of Physics, Royal Institute of Technology (KTH), AlbaNova, SE-106 91 Stockholm, Sweden
[38] Science Institute, University of Iceland, IS-107 Reykjavik, Iceland
[39] College of Science, Ibaraki University, 2-1-1, Bunkyo, Mito 310-8512, Japan
[40] Research Institute for Science and Engineering, Waseda University, 3-4-1, Okubo, Shinjuku, Tokyo 169-8555, Japan

[41] Department of Astronomy, Stockholm University, SE-106 91 Stockholm, Sweden

[42] Yukawa Institute for Theoretical Physics, Kyoto University, Kitashirakawa Oiwake-cho, Sakyo-ku, Kyoto 606-8502, Japan

[43] Université Bordeaux 1, CNRS/IN2p3, Centre d'Études Nucléaires de Bordeaux Gradignan, F-33175 Gradignan, France

[44] Max-Planck Institut für extraterrestrische Physik, D-85748 Garching, Germany

[45] Department of Physics and Department of Astronomy, University of Maryland, College Park, MD 20742, USA

[46] Center for Research and Exploration in Space Science and Technology (CRESST) and NASA Goddard Space Flight Center, Greenbelt, MD 20771, USA

[47] Istituto Nazionale di Fisica Nucleare, Sezione di Roma "Tor Vergata," I-00133 Roma, Italy

[48] Department of Physics, Boise State University, Boise, ID 83725, USA

[49] Institute of Space and Astronautical Science, JAXA, 3-1-1 Yoshinodai, Chuo-ku, Sagamihara, Kanagawa 252-5210, Japan

[50] Hiroshima Astrophysical Science Center, Hiroshima University, Higashi-Hiroshima, Hiroshima 739-8526, Japan

[51] Department of Physics and Astronomy, University of Denver, Denver, CO 80208, USA

[52] Max-Planck-Institut für Physik, D-80805 München, Germany

[53] Santa Cruz Institute for Particle Physics, Department of Physics and Department of Astronomy and Astrophysics,
University of California at Santa Cruz, Santa Cruz, CA 95064, USA

[54] Institut für Astro- und Teilchenphysik and Institut für Theoretische Physik, Leopold-Franzens-Universität Innsbruck, A-6020 Innsbruck, Austria

[55] Department of Physics, University of Washington, Seattle, WA 98195-1560, USA

[56] NYCB Real-Time Computing Inc., Lattingtown, NY 11560-1025, USA

[57] Department of Chemistry and Physics, Purdue University Calumet, Hammond, IN 46323-2094, USA

[58] Institut für Theoretische Physik and Astrophysik, Universität Würzburg, D-97074 Würzburg, Germany

[59] Institució Catalana de Recerca i Estudis Avançats (ICREA), Barcelona, Spain

[60] Consorzio Interuniversitario per la Fisica Spaziale (CIFS), I-10133 Torino, Italy

[61] INTEGRAL Science Data Centre, CH-1290 Versoix, Switzerland

[62] Dipartimento di Fisica, Università di Roma "Tor Vergata," I-00133 Roma, Italy

ABSTRACT

We report an analysis of the interstellar γ-ray emission from the Chamaeleon, R Coronae Australis (R CrA), and Cepheus and Polaris flare regions with the *Fermi* Large Area Telescope. They are among the nearest molecular cloud complexes, within $\sim$300 pc from the solar system. The γ-ray emission produced by interactions of cosmic rays (CRs) and interstellar gas in those molecular clouds is useful to study the CR densities and distributions of molecular gas close to the solar system. The obtained γ-ray emissivities above 250 MeV are $(5.9 \pm 0.1_{\mathrm{stat}}\,{}^{+0.9}_{-1.0}\mathrm{sys}) \times 10^{-27}$ photons s^{-1} sr^{-1} H-atom^{-1}, $(10.2 \pm 0.4_{\mathrm{stat}}\,{}^{+1.2}_{-1.7}\mathrm{sys}) \times 10^{-27}$ photons s^{-1} sr^{-1} H-atom^{-1}, and $(9.1 \pm 0.3_{\mathrm{stat}}\,{}^{+1.5}_{-0.6}\mathrm{sys}) \times 10^{-27}$ photons s^{-1} sr^{-1} H-atom^{-1} for the Chamaeleon, R CrA, and Cepheus and Polaris flare regions, respectively. Whereas the energy dependences of the emissivities agree well with that predicted from direct CR observations at the Earth, the measured emissivities from 250 MeV to 10 GeV indicate a variation of the CR density by $\sim$20% in the neighborhood of the solar system, even if we consider systematic uncertainties. The molecular mass calibrating ratio, $X_{\mathrm{CO}} = N(\mathrm{H_2})/W_{\mathrm{CO}}$, is found to be $(0.96 \pm 0.06_{\mathrm{stat}}\,{}^{+0.15}_{-0.12}\mathrm{sys}) \times 10^{20}$ H$_2$-molecule cm^{-2} (K km s^{-1})$^{-1}$, $(0.99 \pm 0.08_{\mathrm{stat}}\,{}^{+0.18}_{-0.10}\mathrm{sys}) \times 10^{20}$ H$_2$-molecule cm^{-2} (K km s^{-1})$^{-1}$, and $(0.63 \pm 0.02_{\mathrm{stat}}\,{}^{+0.09}_{-0.07}\mathrm{sys}) \times 10^{20}$ H$_2$-molecule cm^{-2} (K km s^{-1})$^{-1}$ for the Chamaeleon, R CrA, and Cepheus and Polaris flare regions, respectively, suggesting a variation of X_{CO} in the vicinity of the solar system. From the obtained values of X_{CO}, the masses of molecular gas traced by W_{CO} in the Chamaeleon, R CrA, and Cepheus and Polaris flare regions are estimated to be $\sim$5 $\times 10^3$ $M_\odot$, $\sim$10^3 $M_\odot$, and $\sim$3.3 $\times 10^4$ $M_\odot$, respectively. A comparable amount of gas not traced well by standard H I and CO surveys is found in the regions investigated.

Key words: cosmic rays – gamma rays: ISM

Online-only material: color figures

1. INTRODUCTION

Observations of high-energy γ-ray emission ($E \gtrsim 30$ MeV) from molecular clouds can be used to study the cosmic-ray (CR) production, the CR density, and the distribution of the interstellar medium (ISM) in such systems. γ-rays are produced in the ISM by interactions of high-energy CR protons and electrons with the interstellar gas, via nucleon–nucleon collisions, electron bremsstrahlung, and inverse Compton (IC) scattering. Since the γ-ray production cross section is almost independent of the chemical or thermodynamic state of the ISM, and the interstellar gas is essentially transparent to those high-energy photons, observations in γ-rays have been recognized as a powerful

probe of the distribution of interstellar matter. If the gas column densities are estimated with good accuracy by observations in other wavebands such as radio, infrared, and optical, then the CR spectrum and density distributions can be examined as well. Molecular clouds that are within 1 kpc from the solar system (namely, nearby molecular clouds) and have masses greater than a few 10^3 $M_\odot$ are well suited for an analysis of their γ-ray emission to investigate the distribution of CR densities and interstellar gas since they are observed at high latitudes and therefore largely free from confusion with the strong emission from the Galactic plane. Study of such nearby molecular clouds in γ-rays can be dated back to the COS-B era (e.g., Bloemen et al. 1984) and was advanced by the EGRET on board the *Compton Gamma-Ray Observatory* (e.g., Hunter et al. 1994). Although some important information has been obtained on properties of CRs and the ISM by these early observations, detailed studies have only been performed on giant molecular clouds with masses greater than $\sim 10^5$ $M_\odot$ such as the Orion

complex (e.g., Digel et al. 1999). The data above 1 GeV, which are crucial to study CR nuclei spectra, suffered from the limited photon statistics, angular resolution, and energy coverage of these early missions.

The advent of the *Fermi Gamma-ray Space Telescope* launched in 2008 has improved the situation significantly. The sensitivity of the Large Area Telescope (LAT) on board *Fermi* is more than an order of magnitude better than that of the EGRET, and enables resolving more point sources and studying the diffuse γ-ray emission with unprecedented sensitivity. In addition, newer surveys of the ISM (e.g., Dame et al. 2001; Kalberla et al. 2005; Grenier et al. 2005) allow us to investigate the CR spectral and density distributions with better accuracy.

Here, we report a *Fermi* LAT study of diffuse γ-rays from the Chamaeleon, R Coronae Australis (R CrA), and Cepheus and Polaris flare molecular clouds. They are among the nearest ($\lesssim 300$ pc from the solar system) molecular clouds exhibiting star formation activity. Although EGRET observed γ-ray emission associated with the molecular gas in the Chamaeleon region (Grenier et al. 2005), no detailed study of CR and matter distributions for the Chamaeleon and R CrA regions has been performed yet since they have rather small masses ($\lesssim 10^4 M_\odot$, about 1/10 of that of the Orion molecular cloud) and consequently small γ-ray fluxes. We also analyzed in detail the region of the Cepheus and Polaris flares which was included in the *Fermi* LAT study of the second Galactic quadrant (Abdo et al. 2010b). It is located in the direction almost opposite to the Chamaeleon region in the Gould Belt (see, e.g., Perrot & Grenier 2003), therefore we can investigate the distribution of the CR density over several hundred pc but still inside the coherent environment of the Gould Belt. This paper is organized as follows. We first describe the observations as well as the sky model preparation and the data analysis in Section 2, and show the obtained results in Section 3. We then discuss the CR and matter distributions in Section 4 and give conclusions in Section 5.

2. DATA ANALYSIS

2.1. Observations and Data Reduction

The LAT, on board the *Fermi Gamma-ray Space Telescope*, is a pair-tracking detector to study γ-rays from ~ 20 MeV to more than 300 GeV. It consists of an array of 4×4 conversion and tracking modules built with tungsten foils and silicon microstrip detectors to measure the arrival directions of incoming γ-rays and a hodoscopic cesium iodide calorimeter to determine the photon energies. The modules are surrounded by 89 segmented plastic scintillators serving as an anticoincidence detector to reject charged-particle background events. A detailed description of the LAT instrumentation can be found in Atwood et al. (2009) and the on-orbit calibration is discussed in Abdo et al. (2009a).

Science operations with the LAT started on 2008 August 4. For this analysis, we have accumulated events obtained from 2008 August 4 to 2010 May 9. During this time interval, the LAT was operated in sky survey mode nearly all of the time and scanned the γ-ray sky with relatively uniform exposure over time (within 10% in regions studied). We used the standard LAT analysis software, Science Tools[67] version v9r16p0 and the response function P6_V3_DIFFUSE, which was developed to account for the detection inefficiencies due to pile-up

and accidental coincidence of events (Rando et al. 2009). We applied the following event selection criteria to the γ-ray events: (1) events must satisfy the standard low-background event selection (so-called diffuse class events; Atwood et al. 2009), (2) the reconstructed zenith angles of the arrival direction of photons are less than $100°$ in order to reduce contamination of photons from the bright Earth rim, and (3) the center of the LAT field of view is within $52°$ from the zenith direction of the sky, in order to exclude the data obtained during the relatively short time intervals of pointed observations when the rocking angle of the LAT was larger. The exposure maps were generated with the same $100°$ limit on zenith angle for each direction in the sky.

The count maps obtained ($E > 250$ MeV) in the Chamaeleon, R CrA, and Cepheus and Polaris flare regions are shown in Figure 1: we set the lower energy limit at 250 MeV to utilize good angular resolution (68% containment radius is $\lesssim 1°5$ above 250 MeV) and the upper energy limit at 10 GeV because of limited photon statistics. We also show positions of point sources with high significance (test statistic, TS,[68] greater than 50) and 2.6 mm carbon-monoxide CO line intensities on the maps. The yellow square indicates the region of interest (ROI) analyzed for each of the regions. In order to take into account the spillover from point sources outside of the ROIs, we also included point sources lying just outside ($\lesssim 5°$) of the region boundaries. Contamination due to the diffuse emission from the interstellar gas outside of the ROIs is also taken into account through the convolution of maps larger than the ROIs.

2.2. Model Preparation

Since the ISM is optically thin to γ-rays in the energy range considered in the paper and the CR spectrum is not expected to vary significantly within small regions, the γ-ray intensity from CR protons and electrons interacting with the interstellar gas may be modeled as a sum of emission from separate gas phases (e.g., Lebrun et al. 1983). This approach has been successfully applied in recent studies of diffuse γ-rays by the LAT (e.g., Abdo et al. 2010b; Ackermann et al. 2011). We followed this method and prepared template maps as described below.

2.2.1. H I and CO Maps

We calculated the column densities $N(\mathrm{H\,I})$ of atomic hydrogen from the Leiden/Argentine/Bonn Galactic H I survey by Kalberla et al. (2005). The optical depth correction of the H I gas is applied under the assumption of a uniform spin temperature $T_S = 125$ K, the value which has often been used in previous studies (e.g., Abdo et al. 2009c, 2010b). This choice of T_S allows us to directly compare our results with other studies. In order to evaluate systematic uncertainties due to the optical depth correction, we also tried several different choices of T_S as described in Section 3. We note that the true T_S is likely not to be uniform even in small regions like the ones we are studying, but exploring a non-uniform T_S is beyond the scope of this paper. We separated the H I column densities in two regions along the line of sight; one corresponds to the local region ($\lesssim 300$ pc) to take into account the ambient atomic gas surrounding the molecular cloud, and the other corresponds to the rest to take into account the remaining gas along the line of sight. From the velocity distribution of the CO emission which traces the molecular cloud, we determined the boundary as shown in

---

[68] TS is defined as TS $= 2(\ln L - \ln L_0)$, where L and L_0 are the maximum likelihoods obtained with and without the source included in the model fitting, respectively; see Mattox et al. (1996).
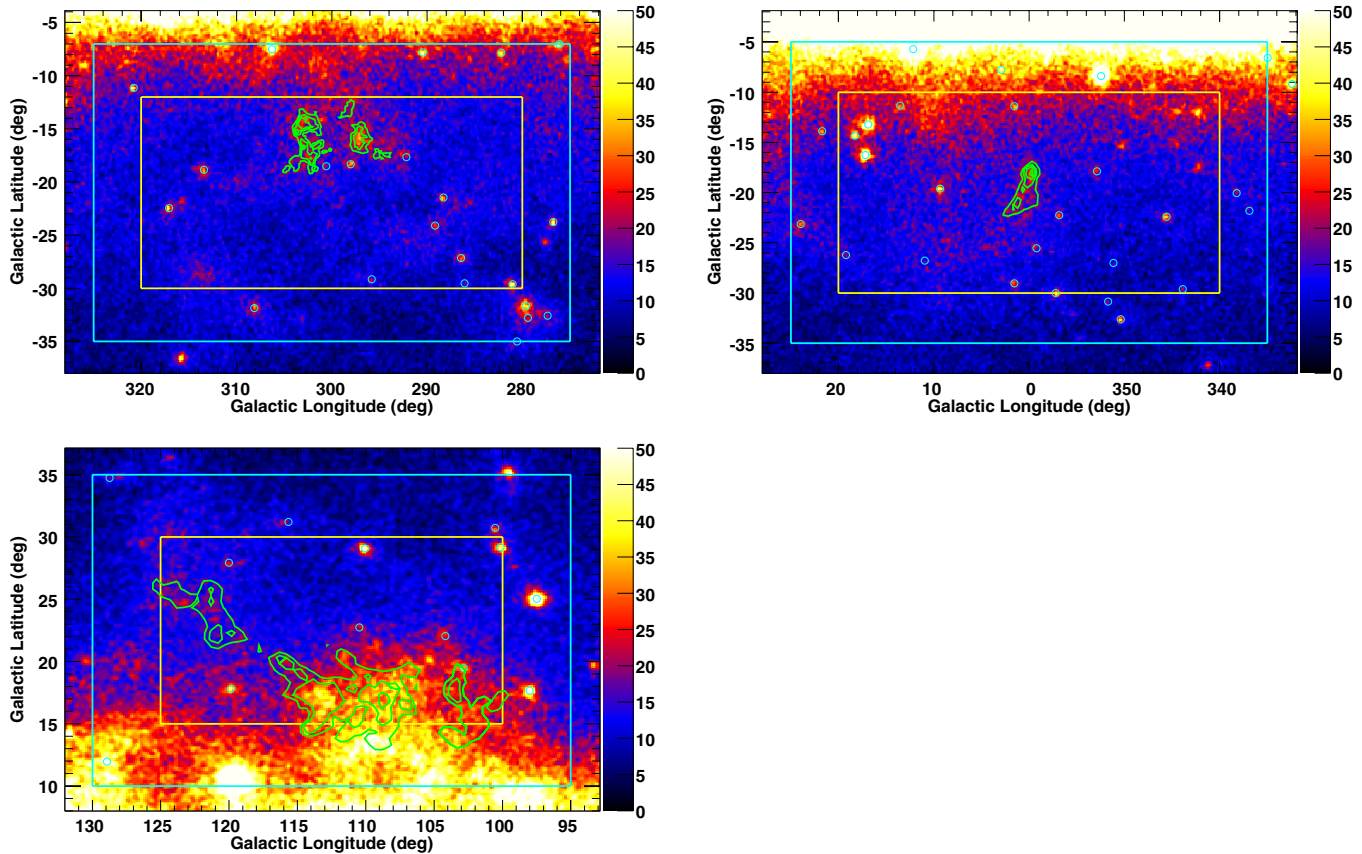
Figure 1. γ-ray count maps above 250 MeV for the Chamaeleon (top left), R CrA (top right), and Cepheus and Polaris flare (bottom left) regions, smoothed with a Gaussian of a standard deviation $\sigma = 0°.5$ for display. The contours indicate intensities W_{CO} of the 2.6 mm line of CO (with the levels of 4, 8, 12, and 16 K km s^{-1}) by Dame et al. (2001), as a standard tracer of the molecular gas. Cyan circles show the positions of point sources with high significance (TS $\geqslant$ 50) in the First *Fermi* LAT catalog (1FGL) by Abdo et al. (2010a). The yellow squares indicate the ROI analyzed for each of the regions. Point sources outside of this ROI but inside the cyan square are taken into account in the analysis.

(A color version of this figure is available in the online journal.)

Figure 2. The local velocity range is $-10 < v_{LSR} < 15$ km s^{-1} for the Chamaeleon region and $-15 < v_{LSR} < 15$ km s^{-1} for the R CrA region for $b > -10°$. Below $-10°$, $|v_{LSR}|$ is increased to 80 km s^{-1} at $b = -20°.5$ in both regions, since the H I gas at such high latitude is likely to be local. The obtained $N(H I)$ maps are shown in the top panels of Figures 3 and 4 for the Chamaeleon region and the R CrA region, respectively. For the Cepheus and Polaris flare region, the cut falls in between the Gould Belt lines and the Local arm lines at -8 km s^{-1} at $b < 15°$, and then opens up to -100 km s^{-1} at $b = 24°$. Since the amount of H I gas in the Local arm and beyond is comparable to that in the Gould Belt for the Cepheus and Polaris flare region in $15° < b < 20°$ (see also Figure 5), using two H I template maps is crucial. For the Chamaeleon and the R CrA regions, the non-local H I gas is almost negligible.

The integrated intensities of the 2.6 mm line, W_{CO}, have been derived from the composite survey of Dame et al. (2001). We used this W_{CO} map as a standard molecular-gas tracer. For better signal-to-noise ratio, the data have been filtered with the moment-masking technique (Dame 2011) to reduce the noise while keeping the resolution of the original data. Since most of the molecular gas turned out to be local according to our velocity cuts, we used only the local CO map in the γ-ray analysis.

2.2.2. Excess Av Map

Dust is a commonly used tracer of the neutral interstellar gas. By comparing the γ-ray observations by EGRET with radio surveys and the dust thermal emission, Grenier et al. (2005) reported a considerable amount of gas at the interface between the atomic/molecular phases in the solar neighborhood, associated with cold dust but not properly traced by H I and CO surveys. This finding was confirmed by dedicated analyses of the diffuse γ-ray emission with the *Fermi* LAT (Abdo et al. 2010b; Ackermann et al. 2011). In order to take into account this additional interstellar gas, we constructed visual extinction (Av) maps, based on the extinction maps derived by Schlegel et al. (1998) from *IRAS* and *COBE* DIRBE data. The Av map on the assumption of a constant gas-to-dust ratio provides an estimate of the total column densities. After fitting a linear combination of the $N(H I)$ and W_{CO} maps through a minimum sum-of-square-residuals criterion in each ROI separately, we thus obtained a residual extinction map, Av$_{res}$ map, accounting for the additional gas which is not properly traced by the H I and CO surveys. Negative residuals are likely to be due to the fluctuation of the original Av map. For simplicity, we clipped data around 0 in the Av$_{res}$ map.

We present gas maps used for the analysis of the Chamaeleon, R CrA, and Cepheus and Polaris flare regions in Figures 3–5, respectively.

2.2.3. IC, Point Sources, and Isotropic Component

In addition to the gas-related components described above, we also need to take into account γ-rays from IC scattering, contributions of point sources, extragalactic diffuse emission,
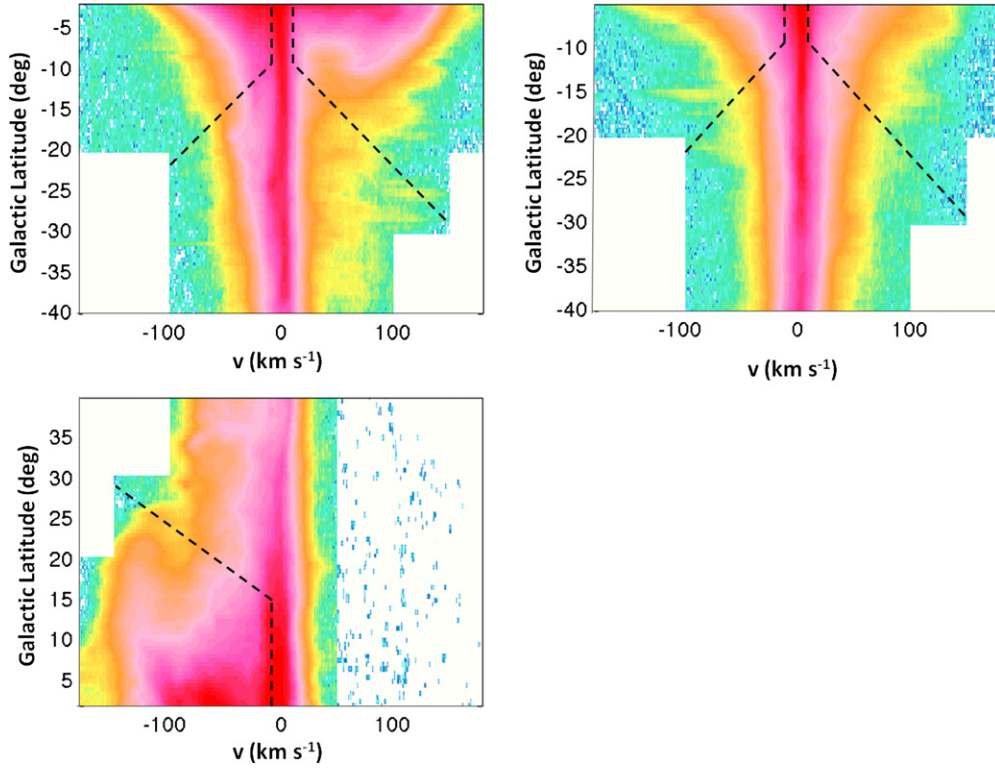
Figure 2. Latitude–velocity diagrams of the intensity of the 21 cm line (log scale in atom cm^{-2}) for the Chamaeleon (top left), R CrA (top right), and Cepheus and Polaris flare (bottom left) regions. The dashed lines indicate the region boundary between the local region ($\lesssim$300 pc) and the rest.

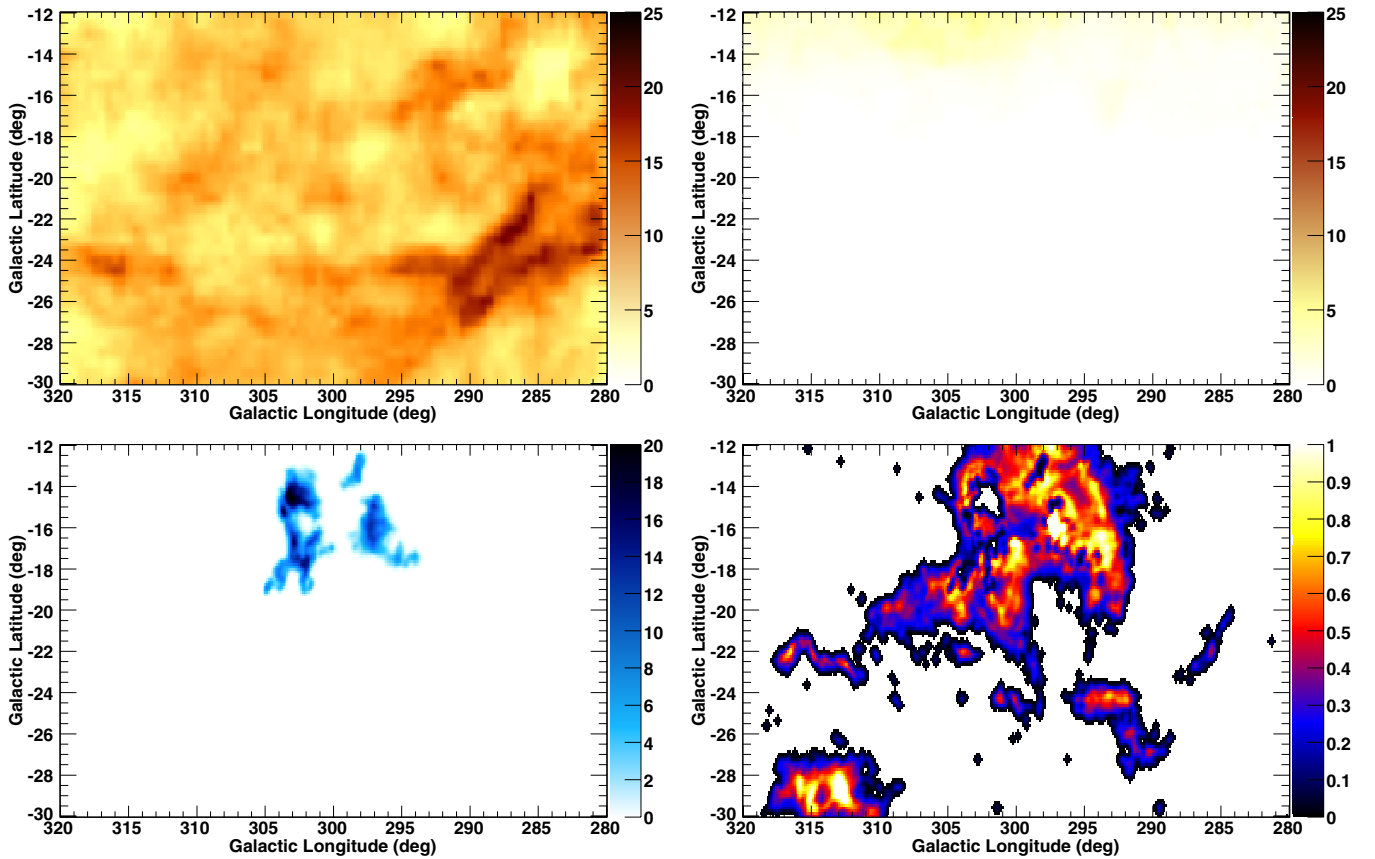(A color version of this figure is available in the online journal.)

Figure 3. Template gas maps for the Chamaeleon region; $N(\mathrm{H\,I})$ (local, top left) and $N(\mathrm{H\,I})$ (non-local, top right) in units of 10^{20} H-atoms cm^{-2}, W_{CO} (bottom left) in units of K km s^{-1}, and $A v_{\mathrm{res}}$ (bottom right) in units of magnitudes. The two $N(\mathrm{H\,I})$ maps have been smoothed with a Gaussian of a standard deviation $\sigma = 1°$ for display while the other two maps have been smoothed with a Gaussian of $\sigma = 0°.25$ in order to keep fine structures seen in W_{CO} and $A v_{\mathrm{res}}$ distributions.

(A color version of this figure is available in the online journal.)

5
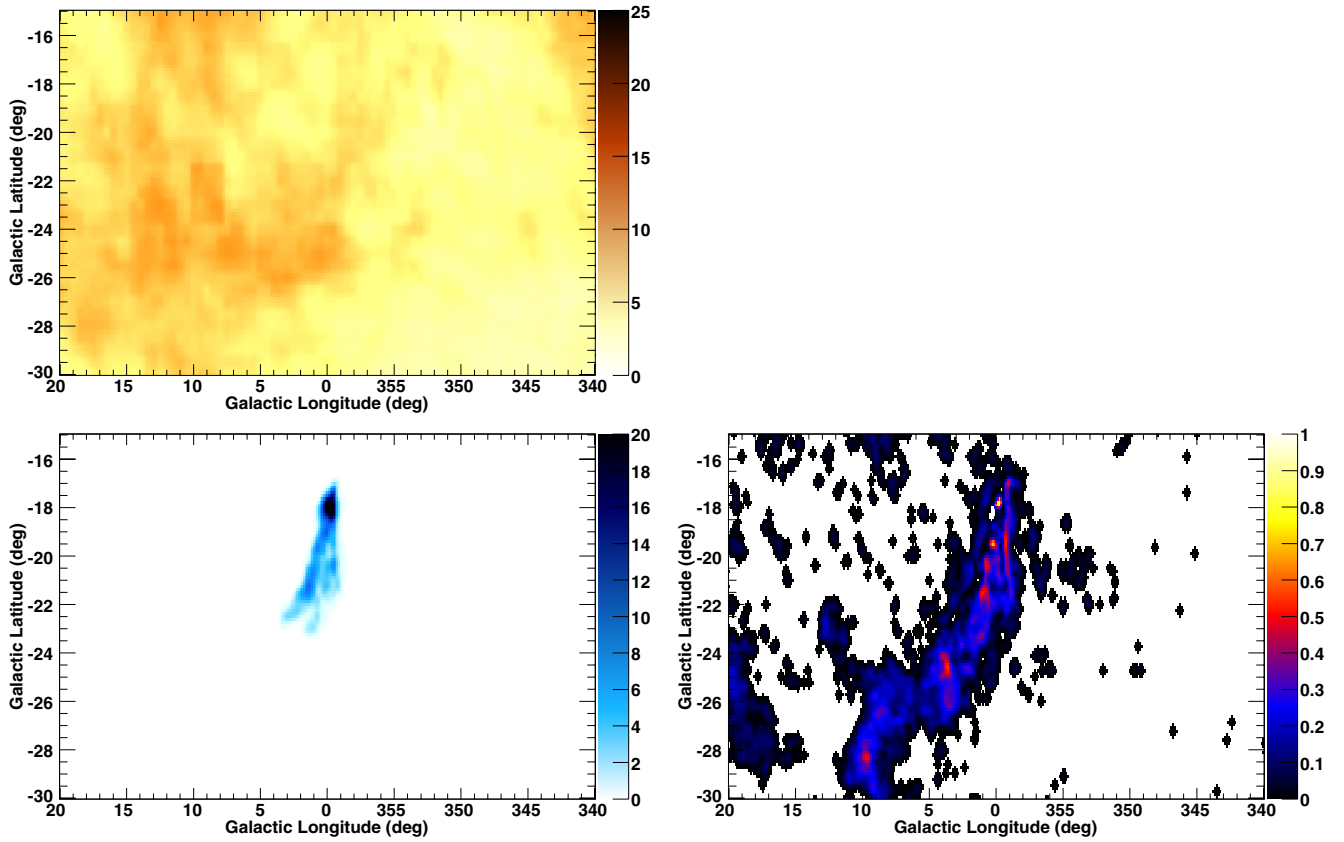
Figure 4. Template gas maps for the R CrA region; $N(\mathrm{H\,I})$ (local, top left) in units of 10^{20} atoms cm^{-2}, W_{CO} (bottom left) in units of K km s^{-1}, and $A\mathrm{v}_{res}$ (bottom right) in units of magnitudes. They have been smoothed in the same way as the maps in Figure 3. The non-local $N(\mathrm{H\,I})$ is almost 0 in our ROI and hence is not shown here. (A color version of this figure is available in the online journal.)

and instrumental residual background. To model the IC emission, we used GALPROP (e.g., Strong & Moskalenko 1998), a numerical code which solves the CR transport equation within our Galaxy and predicts the γ-ray emission produced via interactions of CRs with the ISM. IC emission is calculated from the distribution of propagated electrons and the radiation field model developed by Porter et al. (2008). Here, we adopt the IC model map produced in the GALPROP run 54_77Xvarh7S[69] as a baseline model, in which the CR electron spectrum is adjusted based on the *Fermi* LAT measurement. In this model, the CR source distribution model is adjusted to the LAT data, and is somewhat more concentrated to the inner Galaxy than the pulsar distribution by Lorimer (2004). To take into account uncertainties of the CR electron spectrum and radiation field on the Galactic scale, we set the normalization of this IC component free in each energy bin when we perform the fit (see Section 2.3). In order to evaluate the systematic uncertainty due to IC models, we also tried four other models, which are constructed under different assumptions about the distribution of CR sources such as supernova remnants (Case & Bhattacharya 1998) and pulsars (Lorimer 2004), and intensity of the interstellar radiation field depending on the input luminosity of the Galactic bulge component (e.g., Ackermann et al. 2012).

To take into account γ-ray point sources, we used the 1FGL catalog based on the first 11 months of the science phase of the mission (Abdo et al. 2010a). We included in our analysis point sources detected with TS $\geqslant$ 50 in the 1FGL catalog and other significant point sources included in the 2FGL catalog as described in Section 2.3.

To represent the sum of the extragalactic diffuse emission and the residual background from the misclassified CR interactions in the LAT, we adopted a publicly available isotropic spectrum[70] obtained by a fit to emission from the high-latitude sky ($b >$ 30°). This component is fixed in our analysis. The uncertainty due to this isotropic term will be discussed in Section 3.

2.3. Analysis Procedure

With the usual assumptions of optical thinness and that CRs uniformly thread the ISM, γ-ray intensity $I_\gamma(l, b)$ (s^{-1} cm^{-2} sr^{-1} MeV^{-1}) at a given energy can be modeled as

$$I_\gamma(l, b) = \sum_{i=1}^{2} q_{\mathrm{H\,I},i} \cdot N(\mathrm{H\,I})(l, b)_i + q_{CO} \cdot W_{CO}(l, b)$$
$$+ q_{Av} \cdot A\mathrm{v}_{res}(l, b) + c_{IC} \cdot I_{IC}(l, b) + I_{iso} + \sum_{j} \mathrm{PS}_j,$$
(1)

where sum over i represents the two regions (local and non-local regions), $q_{\mathrm{H\,I},i}$ (s^{-1} sr^{-1} MeV^{-1}), q_{CO} (s^{-1} cm^{-2} sr^{-1} MeV^{-1} (K km s^{-1})$^{-1}$), and q_{Av} (s^{-1} cm^{-2} sr^{-1} MeV^{-1} mag^{-1}) are the emissivity per H I atom, per W_{CO} unit, and per $A\mathrm{v}_{res}$ magnitude, respectively. I_{IC} and I_{iso} are the IC model and isotropic background intensities (s^{-1} cm^{-2} sr^{-1} MeV^{-1}), respectively, and PS$_j$ represents contributions of point sources. Hard γ-ray emission with a characteristic bubble shape above and below

---

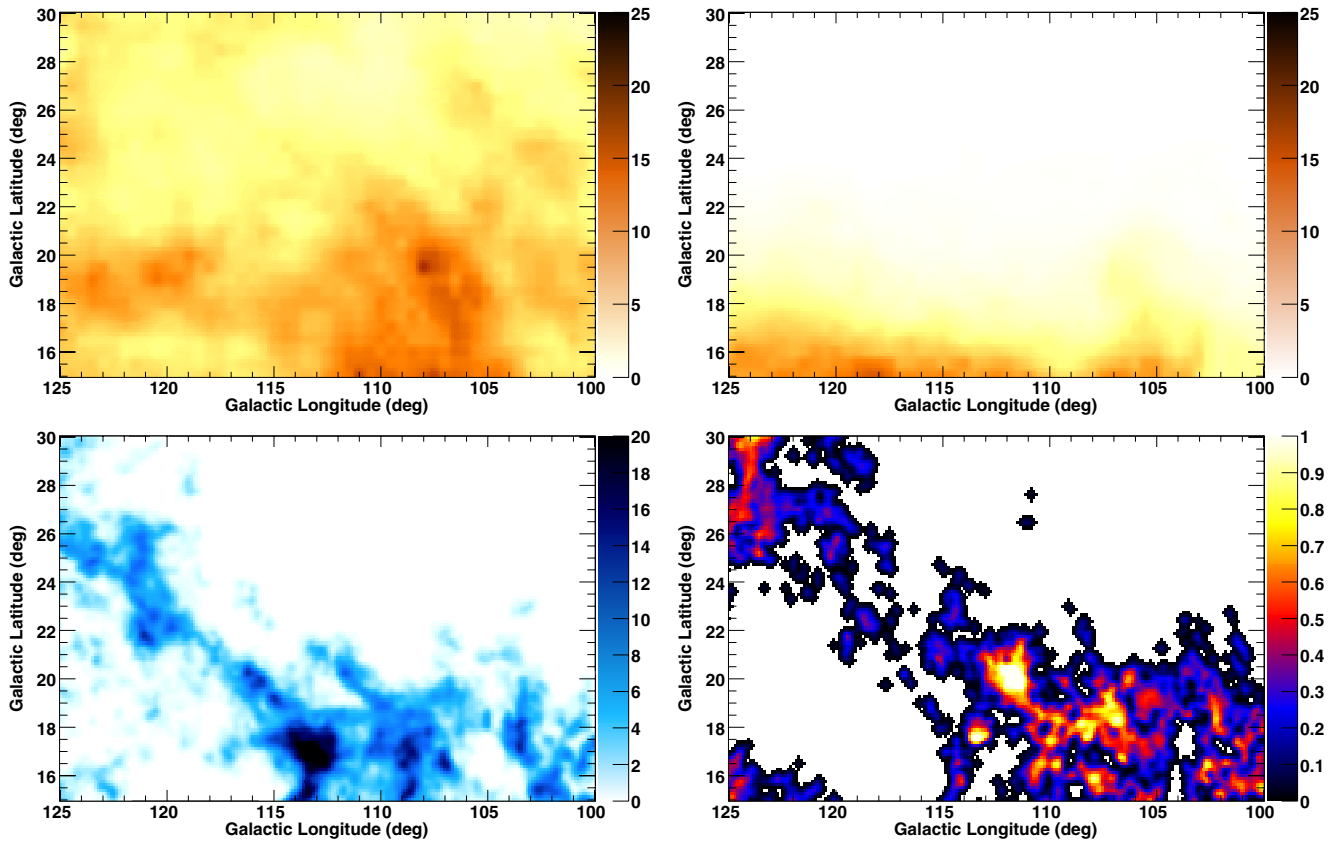**Figure 5.** Template gas maps for the Cepheus and Polaris flare region; N(H I) (local, top left) and N(H I) (non-local, top right) in units of 10^{20} atoms cm^{-2}, W_{CO} (bottom left) in units of K km s^{-1}, and $A_{v_{res}}$ (bottom right) in units of magnitudes. They have been smoothed in the same way as maps in Figure 3.
(A color version of this figure is available in the online journal.)

the Galactic center (usually called the "*Fermi* bubbles") that was found in the *Fermi* LAT data (e.g., Su et al. 2010) has a large spatial extent in the R CrA region. As described below, we found residuals with a hard γ-ray spectrum in the R CrA region, and included an additional template in Equation (1).

The γ-ray data in our ROIs were binned in $0°.25 \times 0°.25$ pixels and fitted with Equation (1) in eight logarithmically equally spaced energy bins from 250 MeV to 10 GeV using a binned maximum likelihood method with Poisson statistics. Low photon statistics and poor angular resolution at low energy ($\sim1°.5$ at 250 MeV under the 68% containment radius) do not allow us to separate components reliably. For convolution of diffuse emission with the instrumental response functions, we assumed an E^{-2} spectrum and the integrated intensities were allowed to vary in each of the eight energy bins. Changing the fixed spectral shape index over the range from -1.5 to -3.0 has negligible effect on the obtained spectrum. Data in the R CrA region with energies above 4 GeV are grouped in a single bin to get larger statistics.

We started the analysis for the Chamaeleon region with point sources detected with high significance (TS $\geqslant 100$) in the 1FGL catalog. The normalizations for each energy bin are allowed to vary for sources inside our ROI. We also included sources lying outside ($\leqslant5°$) ROI, with the spectral parameters fixed to those in the 1FGL catalog. We first fitted the model to LAT data without the $A_{v_{res}}$ map, and then included it and confirmed that the likelihood improved significantly; the test statistic, defined as TS $= 2(\ln L_1 - \ln L_0)$, where $L_0(L_1)$ is the likelihood without(with) additional component, is 704 for eight more free parameters for the energy range from 250 MeV to 10 GeV.
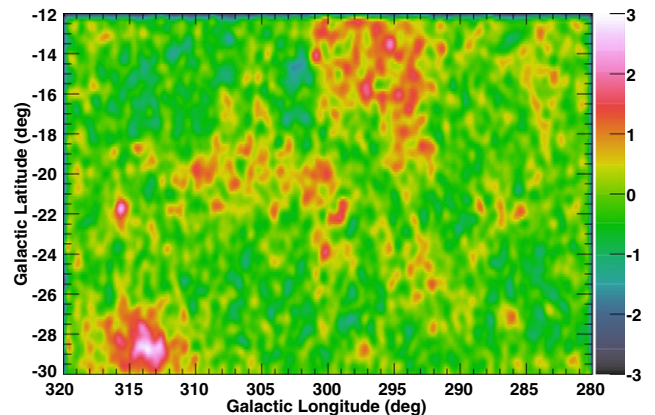

Figure 6. γ-ray residual map obtained from the fit without the $A_{v_{res}}$ map in units of standard deviations above 250 MeV for the Chamaeleon region smoothed with a Gaussian of $\sigma = 0°.5$. Positive residual counts are seen where we have positive $A_{v_{res}}$ (Figure 3).
(A color version of this figure is available in the online journal.)

Figure 6 shows the residual (data minus fitted model) map obtained from the fit without the $A_{v_{res}}$ map. Positive residual counts are seen where we have positive $A_{v_{res}}$ (Figure 3). We thus confirmed that the positive $A_{v_{res}}$ traces the gas not well measured by H I and CO surveys, and included the $A_{v_{res}}$ map in the following analysis. We repeated the same procedure and obtained the same conclusion for the Cepheus and Polaris flare region. In the R CrA region, large residual clumps are still seen around ($0° < l < 15°$) and ($-30° < b < -15°$) even if we included the $A_{v_{res}}$ map as shown by Figure 7, probably due to the
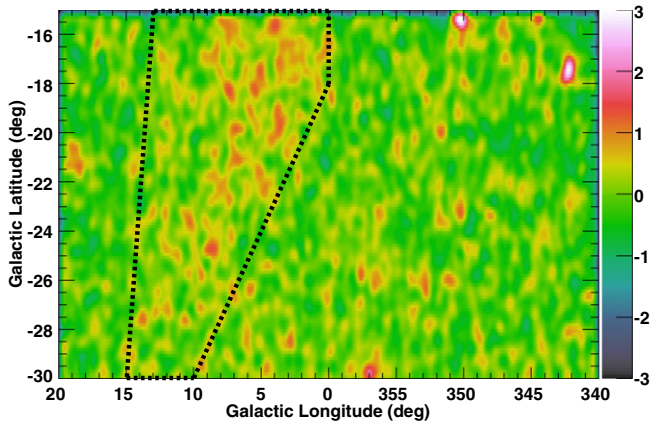
Figure 7. γ-ray residual map obtained from the fit in units of standard deviations above 250 MeV for the R CrA region smoothed with a Gaussian of $\sigma = 0°.5$. Dashed lines indicate region boundaries for the additional flat template map.

(A color version of this figure is available in the online journal.)

southern *Fermi* bubble. In order to account for these residuals, we used a flat template model map with the shape as shown in Figure 7 with a free normalization in each energy bin. We note that the template map is just to accommodate the residuals, not to investigate the *Fermi* bubble. The residuals are improved significantly as shown in the bottom right panel of Figure 9, and the intensity of this template is too low to significantly impact on the local H I gas emissivity as shown in the top right panel of Figure 12.

We then lowered the threshold for point sources down to TS = 50. Although the fit improves in terms of the log-likelihood, the effect on the emissivities associated with gas maps is negligible for the three regions (smaller than the statistical error). However, some point-like excesses corresponding to objects not included in the 1FGL catalog are seen in the R CrA region (2FGL J1830.2−4441, 2FGL J1816.7−4942, and 2FGL J1825.1−5231) and the Cepheus and Polaris flare region (2FGL J2022.5+7614 and 2FGL J2009.7+7225). These may be sources that became luminous after the 1FGL catalog was published. We thus included those sources and confirmed that gas emissivities are almost unaffected while the residual map becomes flatter. We therefore adopted the model described by Equation (1) (plus a flat template for the R CrA region) with point sources with TS $\geqslant$ 50 in the 1FGL catalog (plus additional sources in the R CrA, and Cepheus and Polaris flare regions described above) as our baseline model. We note that an unassociated source in the 1FGL catalog, 1FGL J1903.8−3718c, is located on a CO core of the R CrA molecular cloud and was recognized in the 1FGL catalog as potentially being spurious. We thus did not include this source in our model. We confirmed that the obtained emissivities are almost the same if we mask the region of the CO core.

3. RESULTS

Figures 8–10 show the γ-ray data count maps, fitted model count maps, and the residual maps for the Chamaeleon, R CrA, and Cepheus and Polaris flare regions, respectively, in
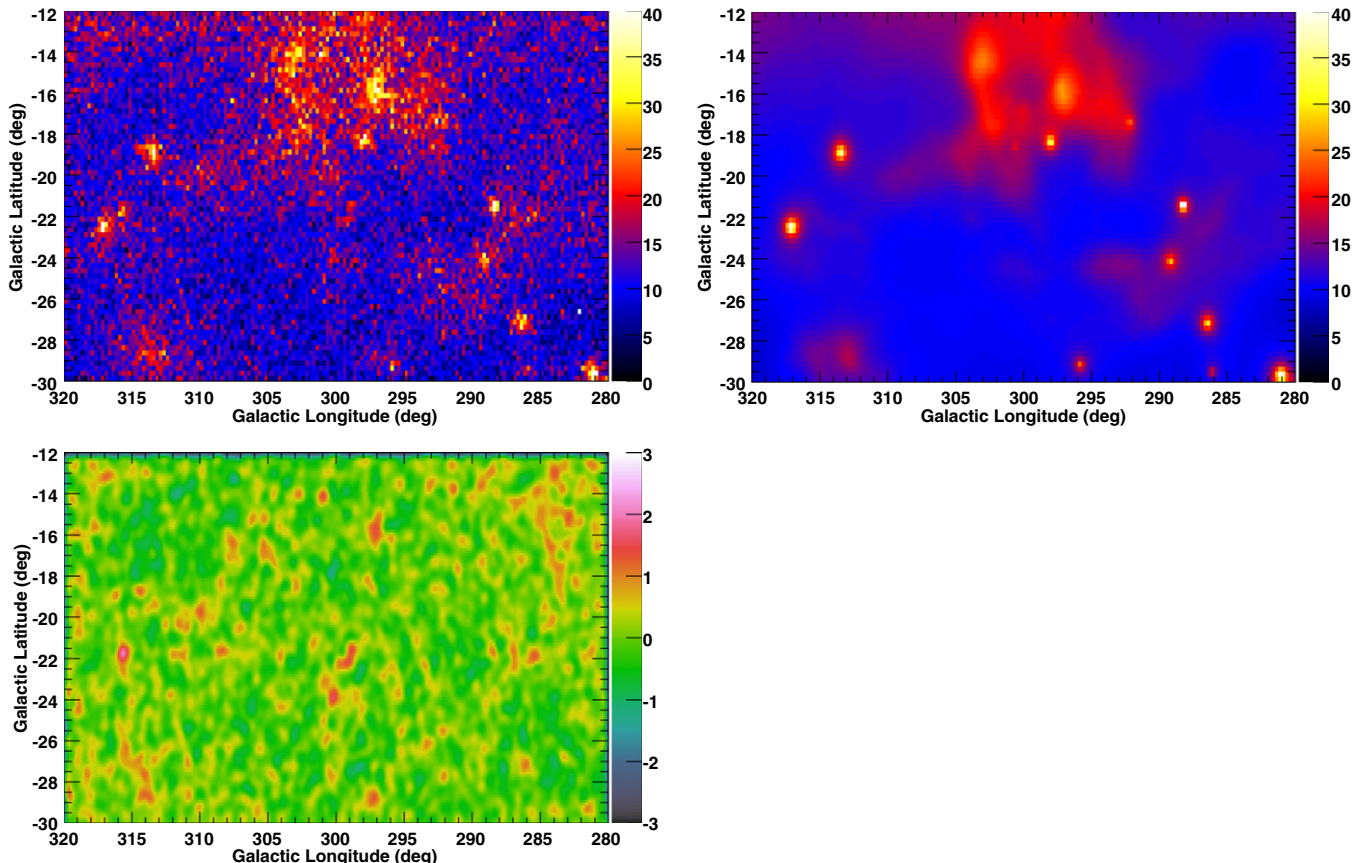

Figure 8. Data count map (top left), fitted model count map (top right), and residual map (bottom left) in units of standard deviations above 250 MeV under the assumption of $T_S = 125$ K for the Chamaeleon region. The residual map has been smoothed with a Gaussian of $\sigma = 0°.5$.

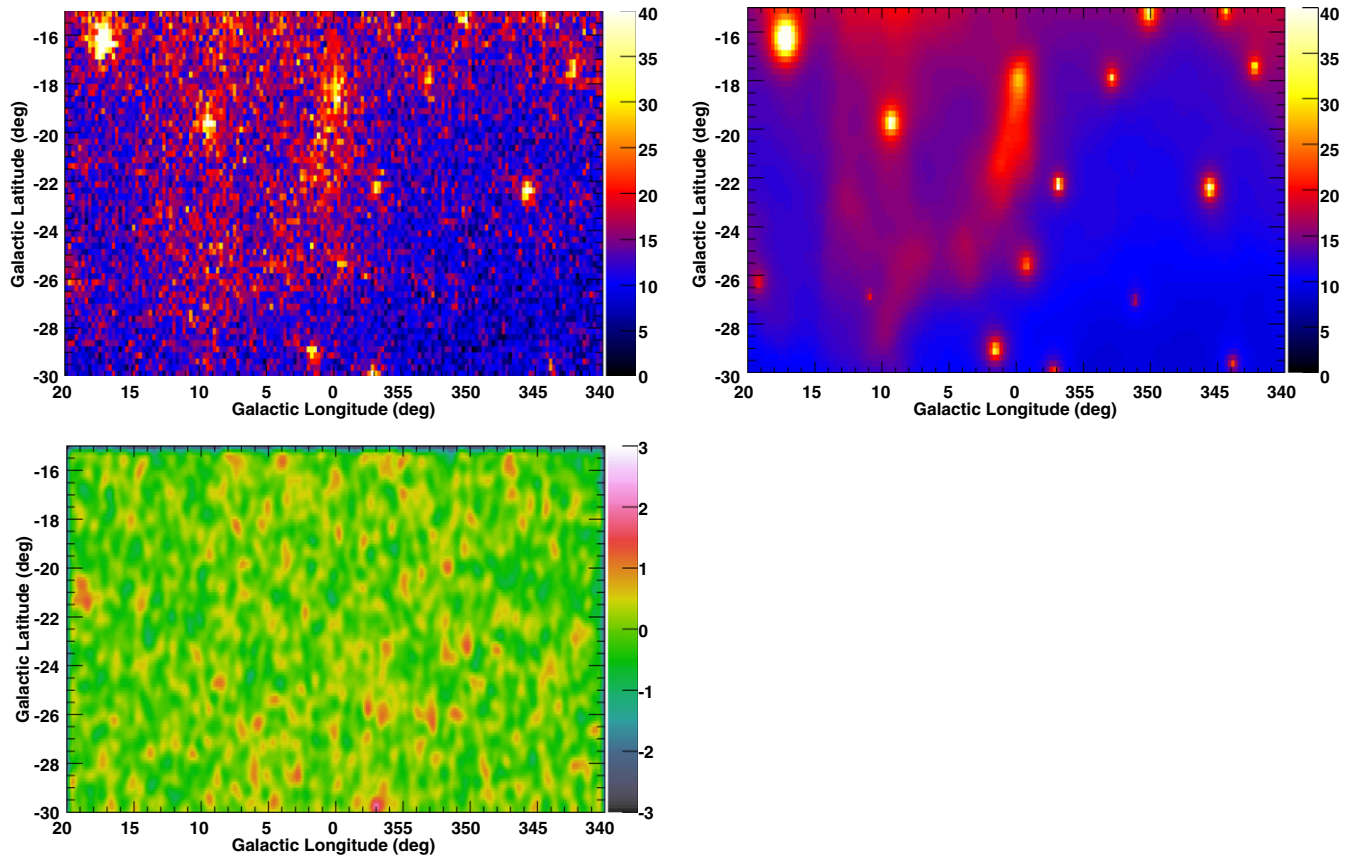(A color version of this figure is available in the online journal.)

Figure 9. Same as Figure 8 for the R CrA region.

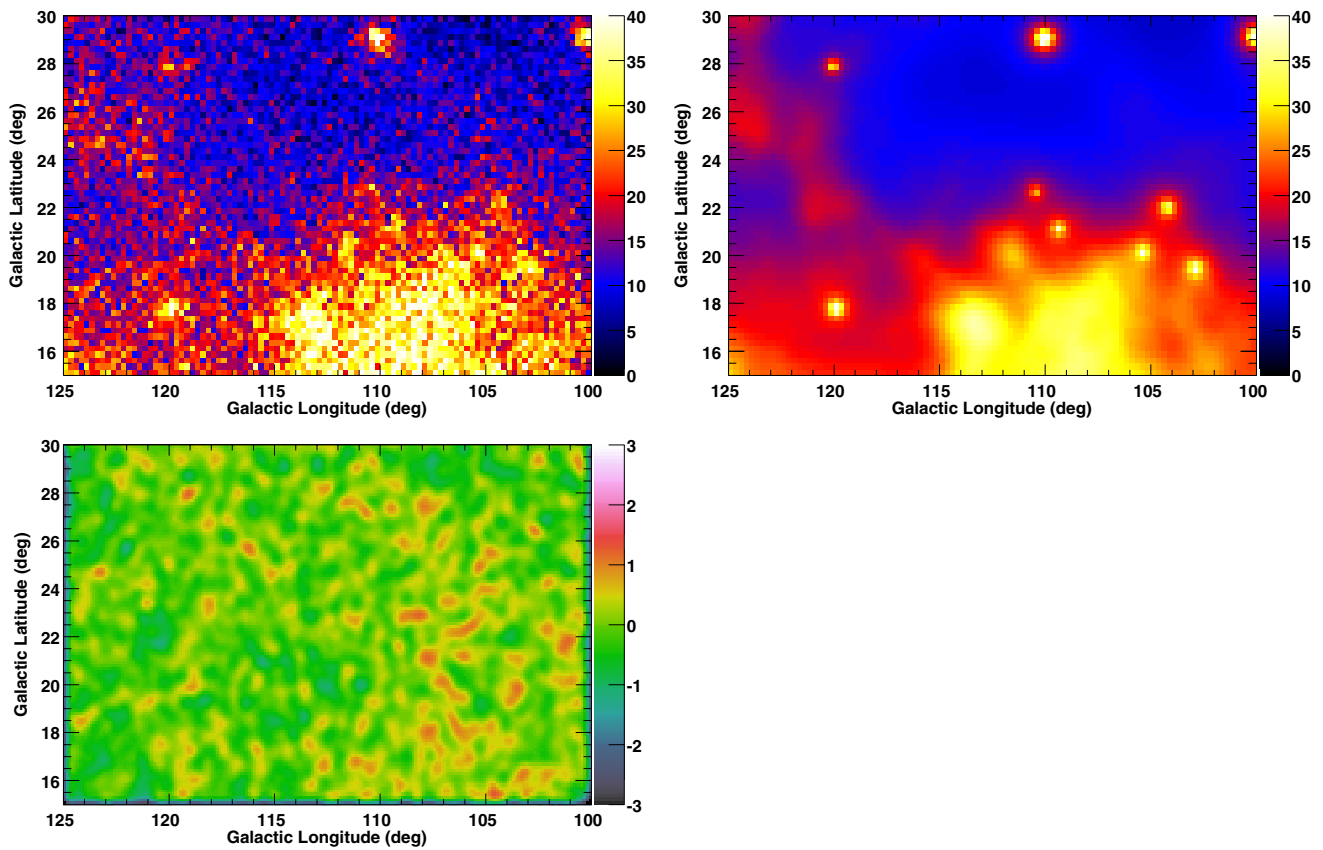(A color version of this figure is available in the online journal.)

Figure 10. Same as Figure 8 for the Cepheus and Polaris flare region.

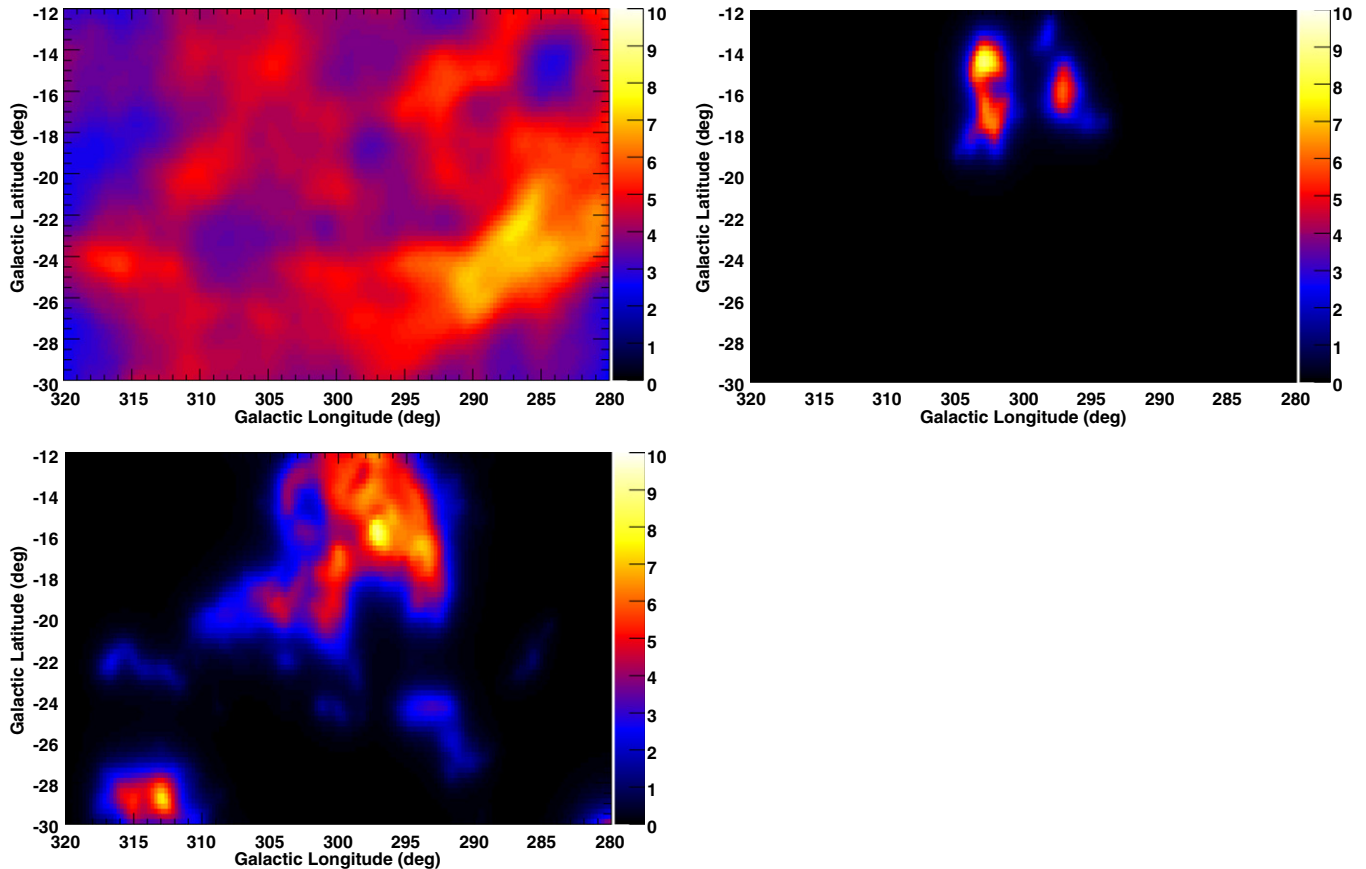(A color version of this figure is available in the online journal.)

9

Figure 11. Fitted model count maps above 250 MeV for the Chamaeleon region; H I component (top left), CO component (top right), and $A v_{\rm res}$ component (bottom left).
(A color version of this figure is available in the online journal.)

which the residuals are expressed in units of approximate standard deviations (square root of the model counts). The residual maps show no conspicuous structures, indicating that our model reasonably reproduces the data, particularly the diffuse emission. For illustrative purposes, we present the fitted model count maps for the Chamaeleon region decomposed into each gas component in Figure 11, in which the γ-ray emission from H I, that from the molecular gas traced by $W_{\rm CO}$, and that inferred from the $A v_{\rm res}$ map are shown. Although the distribution of $N({\rm H\,I})$ is rather uniform in our ROI, it exhibits some structures and allows us to derive the emissivity of the H I gas, which is proportional to the flux of ambient CRs. The distribution of $W_{\rm CO}$ is highly structured and is concentrated in the longitude range from $295°$ to $305°$ and in the latitude range from $-12°$ to $-20°$. The gas traced by $A v_{\rm res}$ lies at the interface between the H I component (atomic gas) and the CO component (molecular gas), and has a mass (proportional to the γ-ray counts) comparable to or larger than that of the molecular gas traced by $W_{\rm CO}$.

Figure 12 shows the fitted spectra for each component. Although the contributions from IC and isotropic components are large, the spectra of each gas component are reliably constrained due to their characteristic spatial distributions as shown in Figures 3–5. The hard spectra of the IC term and the flat template model component of the R CrA region are likely to be due to the southern *Fermi* bubble.

The fit results are summarized in Tables 1–3 for the case of $T_{\rm S} = 125$ K in the Chamaeleon, R CrA, and Cepheus and Polaris flare regions, respectively. The integrated H I emissivity for the

Table 1
Gas Emissivities in the Chamaeleon Regions with Their Statistical Uncertainties (Assuming $T_{\rm S} = 125$ K for the H I Maps Preparation)

Energy (GeV)	$q_{\rm H\,I,1}$	$q_{\rm CO}$	$q_{\rm Av}$
0.25–0.40	2.3 ± 0.1	0.30 ± 0.06	0.57 ± 0.03
0.40–0.63	1.50 ± 0.06	0.33 ± 0.04	0.34 ± 0.02
0.63–1.00	0.99 ± 0.04	0.17 ± 0.02	0.21 ± 0.01
1.00–1.58	0.61 ± 0.03	0.13 ± 0.01	0.125 ± 0.008
1.58–2.51	0.29 ± 0.02	0.069 ± 0.009	0.060 ± 0.006
2.51–3.98	0.13 ± 0.01	0.027 ± 0.006	0.033 ± 0.004
3.98–6.31	0.08 ± 0.01	0.010 ± 0.004	0.014 ± 0.003
6.31–10.00	0.019 ± 0.006	0.007 ± 0.003	0.005 ± 0.002
Total	5.9 ± 0.1	1.04 ± 0.08	1.36 ± 0.04

Notes. Units: $q_{\rm H\,I,1}(10^{-27}\,{\rm s}^{-1}\,{\rm sr}^{-1})$, $q_{\rm CO}(10^{-6}\,{\rm cm}^{-2}\,{\rm s}^{-1}\,{\rm sr}^{-1}\,({\rm K\,km\,s}^{-1})^{-1})$, $q_{\rm Av}(10^{-5}\,{\rm cm}^{-2}\,{\rm s}^{-1}\,{\rm sr}^{-1}\,{\rm mag}^{-1})$.

Chamaeleon region above 250 MeV is $(5.9 \pm 0.1_{\rm stat}\,^{+0.9}_{-1.0}{\rm sys}) \times 10^{-27}$ photons s^{-1} sr^{-1} H-atom^{-1}, and those of the R CrA, and Cepheus and Polaris flare regions are $(10.2 \pm 0.4_{\rm stat}\,^{+1.2}_{-1.7}{\rm sys}) \times 10^{-27}$ photons s^{-1} sr^{-1} H-atom^{-1} and $(9.1 \pm 0.3_{\rm stat}\,^{+1.5}_{-0.6}{\rm sys}) \times 10^{-27}$ photons s^{-1} sr^{-1} H-atom^{-1}, respectively. (See below for the evaluation of the systematic uncertainty from the sky model.)

Figure 13 shows the emissivity spectra of each gas component in the Chamaeleon region under the assumption of $T_{\rm S} = 125$ K. In order to examine the systematic uncertainty due to the optical depth correction, we also tried to fit the data with maps obtained
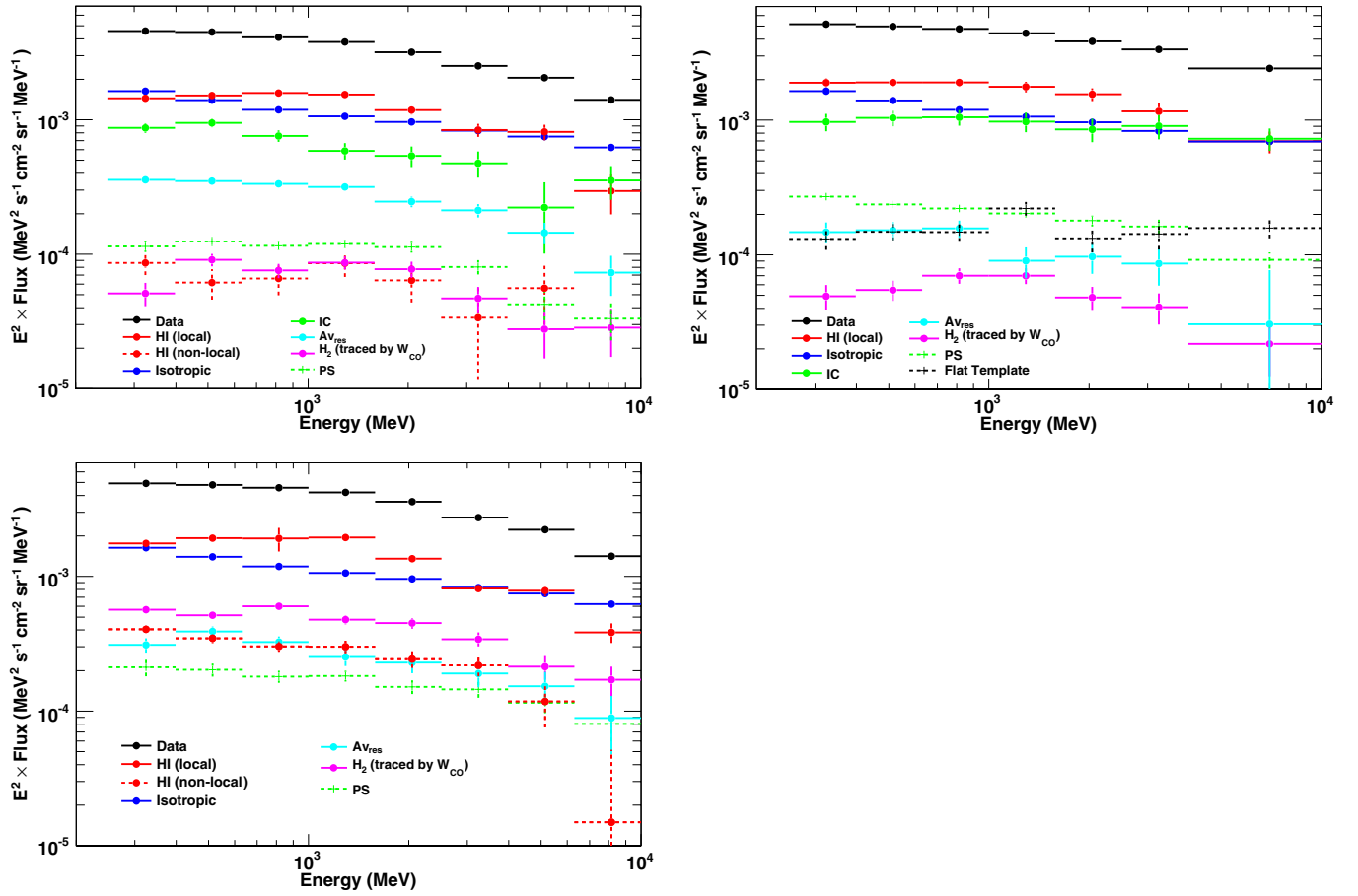
Figure 12. γ-ray spectra of each component (each gas phase, IC, isotropic component, point sources, and flat template model for the R CrA region) for the Chamaeleon (top left), R CrA (top right), and Cepheus and Polaris flare region (bottom left). The H I (non-local) for the R CrA region and the IC component for the Cepheus and Polaris flare are not shown here since they are negligible.

(A color version of this figure is available in the online journal.)

<div style="display:flex">
<div>

Table 2
Same as Table 1 for the R CrA Region

Energy (GeV)	$q_{H I}$	q_{CO}	q_{Av}
0.25–0.40	4.1 ± 0.3	0.7 ± 0.1	1.0 ± 0.2
0.40–0.63	2.6 ± 0.2	0.45 ± 0.08	0.6 ± 0.1
0.63–1.00	1.6 ± 0.1	0.37 ± 0.05	0.41 ± 0.06
1.00–1.58	0.96 ± 0.09	0.23 ± 0.03	0.15 ± 0.04
1.58–2.51	0.53 ± 0.06	0.10 ± 0.02	0.10 ± 0.03
2.51–3.98	0.25 ± 0.04	0.05 ± 0.01	0.06 ± 0.02
3.98–10.00	0.14 ± 0.03	0.019 ± 0.008	0.008 ± 0.001
Total	10.2 ± 0.4	1.9 ± 0.2	2.3 ± 0.2

Notes. Units: $q_{H I}(10^{-27}$ s^{-1} sr^{-1}), $q_{CO}(10^{-6}$ cm^{-2} s^{-1} sr^{-1} (K km s^{-1})$^{-1}$), $q_{Av}(10^{-5}$ cm^{-2} s^{-1} sr^{-1} mag^{-1}).

</div>
<div>

Table 3
Same as Table 1 for the Cepheus and Polaris Flare Region

Energy (GeV)	$q_{H I}$	q_{CO}	q_{Av}
0.25–0.40	3.5 ± 0.1	0.52 ± 0.04	0.53 ± 0.06
0.40–0.63	2.37 ± 0.06	0.29 ± 0.02	0.41 ± 0.04
0.63–1.00	1.6 ± 0.3	0.21 ± 0.01	0.22 ± 0.02
1.00–1.58	0.97 ± 0.03	0.105 ± 0.008	0.11 ± 0.02
1.58–2.51	0.48 ± 0.02	0.061 ± 0.005	0.06 ± 0.01
2.51–3.98	0.20 ± 0.01	0.029 ± 0.003	0.030 ± 0.006
3.98–6.31	0.11 ± 0.01	0.012 ± 0.002	0.016 ± 0.004
6.31–10.00	0.035 ± 0.006	0.006 ± 0.001	0.006 ± 0.003
Total	9.2 ± 0.3	1.23 ± 0.05	1.38 ± 0.08

Notes. Units: $q_{H I}(10^{-27}$ s^{-1} sr^{-1}), $q_{CO}(10^{-6}$ cm^{-2} s^{-1} sr^{-1} (K km s^{-1})$^{-1}$), $q_{Av}(10^{-5}$ cm^{-2} s^{-1} sr^{-1} mag^{-1}).

</div>
</div>

by assuming $T_S = 100$ K and under the approximation that the gas is optically thin. We evaluated the uncertainty of the isotropic component to be ±10% by comparing the model we adopted and those derived in other LAT studies of mid-latitude regions (Abdo et al. 2009b, 2009c). We thus reran the analysis described in Section 2.3 assuming a 10% higher and lower intensity for the fixed isotropic component. We also investigated the effect on the systematic uncertainty due to the IC component by using different IC model maps, as described in Section 2.2.3. The effects of the uncertainty of the T_S, isotropic component, and IC models are quite comparable, therefore we added them. The

obtained systematic uncertainty is comparable to or slightly larger than the statistical error as shown by Figure 13 for $q_{H I}$ (top left panel). On the other hand, the systematic uncertainty of the q_{CO} and q_{Av} is smaller than the statistical error and is not shown in this figure for clarity. The obtained spectra in the R CrA region and the Cepheus and Polaris flare region are summarized in Figures 14 and 15, respectively. We performed the same procedure and evaluated the systematic uncertainties due to the T_S, isotropic component, and IC models as a shaded area in the figures.
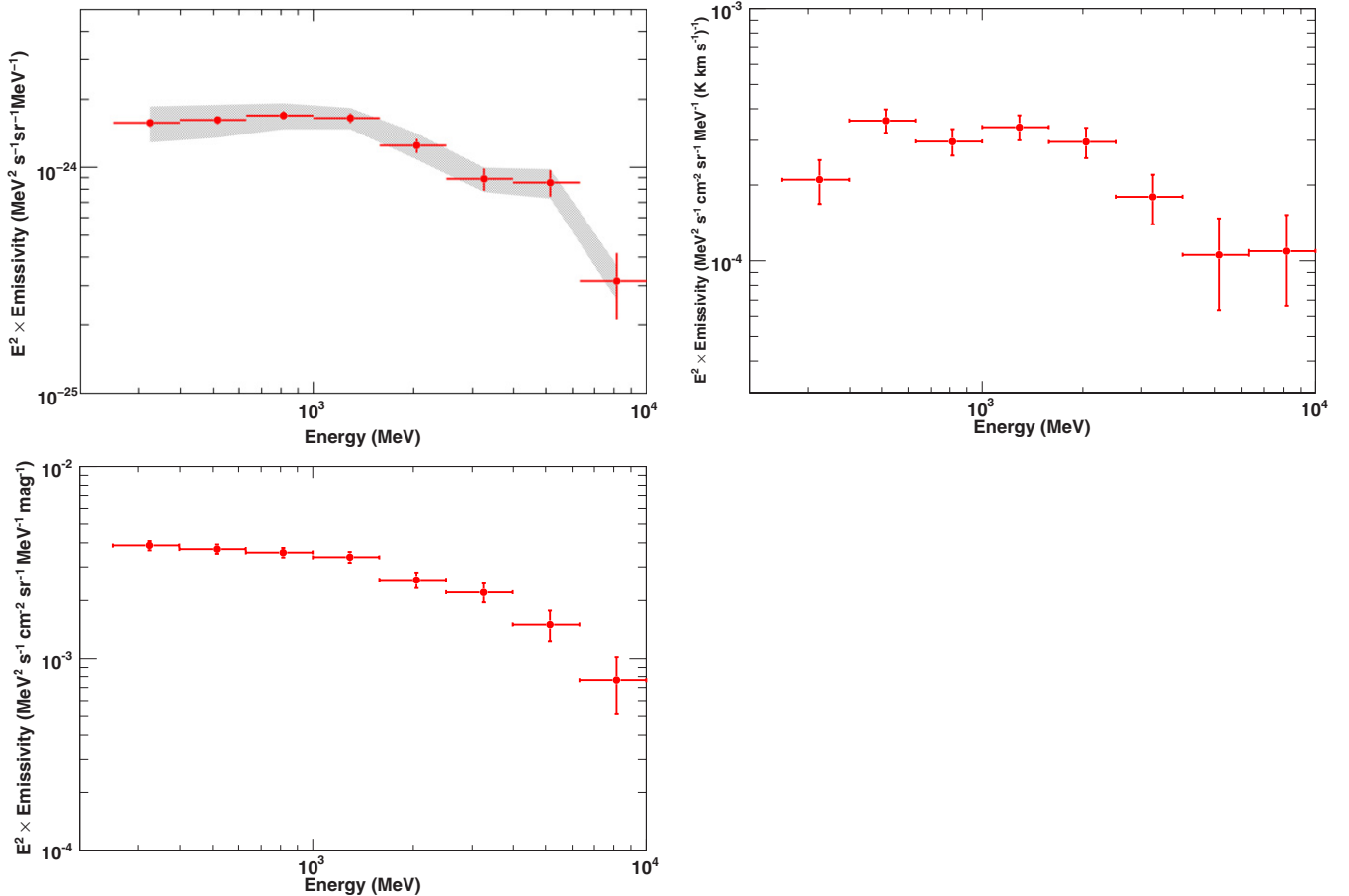
Figure 13. Emissivity spectrum of the local H I gas (top left), that per W_{CO} unit (top right), and that per unit $A_{v_{res}}$ magnitude (bottom left) of the Chamaeleon region. The shaded area shows systematic uncertainties for H I (see the text for details).

(A color version of this figure is available in the online journal.)

Evaluation of the systematic uncertainty is crucial for this study. We therefore performed two more tests.

1. We modified the longitude range from $-20° < l < 20°$ to $-30° < l < 10°$ for the R CrA region, and found that the obtained H I emissivity was lower by ∼10%. This is due to a coupling between the H I and IC components, and we take this effect on the H I emissivity into account in the evaluation of the overall systematic uncertainty.
2. The prominent H I cloud at $280° < l < 295°$ and $-28° < b < -20°$ is not spatially associated with the Chamaeleon molecular cloud, and it may not be physically related to the molecular cloud. We masked this region and found that the H I emissivity is almost unaffected.

The resultant peak-to-peak uncertainty of the local H I emissivity is less than ∼20% across the energy range for three regions investigated.

4. DISCUSSION

4.1. CR Density and Spectrum Close to the Solar System

It is generally believed that supernova remnants are the primary sources of the Galactic CRs. Due to strong selection effects in detecting supernova remnants, their spatial distribution is not well determined. Therefore a smooth, axisymmetric distribution has often been assumed in theoretical calculations, resulting in a smooth decline of CR density as a function of

the Galactocentric radius. This assumption, however, should be tested against observations. In Figure 16, we compare the obtained H I emissivity spectra in the Chamaeleon, R CrA, and Cepheus and Polaris flare regions (for $T_S = 125$ K) and model emissivity spectra[71] for the local interstellar spectrum (LIS) used in Abdo et al. (2009c), based on local direct measurement of CRs. The spectral shapes for the three regions studied here agree well with the LIS models, indicating that the CR nuclei have similar spectral distribution in the vicinity of the solar system. On the other hand, the absolute emissivities differ among regions. The emissivities of the three regions studied differ by ∼50%, estimated from the total q_{HI} shown in Tables 1–3. We note that the systematic uncertainty of the LAT effective area (5% at 100 MeV and 20% at 10 GeV; Rando et al. 2009) does not affect the relative value of emissivities among these regions in Figure 16. Although the emissivities of the R CrA region and the Cepheus and Polaris flare region are comparable, that of the Chamaeleon region is lower by ∼20%, even if we take the systematic uncertainty into account (see Section 3). As a further test, we fixed the emissivity of the Chamaeleon region to that of the model for the LIS with the nuclear enhancement factor of 1.84 and performed the fitting. The fit turns out to

---

[71] The model is calculated from the LIS compatible with the CR proton spectrum measured by Alcaraz et al. (2000) and Sanuki et al. (2000), under the assumption that the nuclear enhancement factors (the correction terms to take into account the contribution from nuclei heavier than protons in both CRs and interstellar matter) are 1.45 and 1.84 (Mori 2009); see Abdo et al. (2009c).
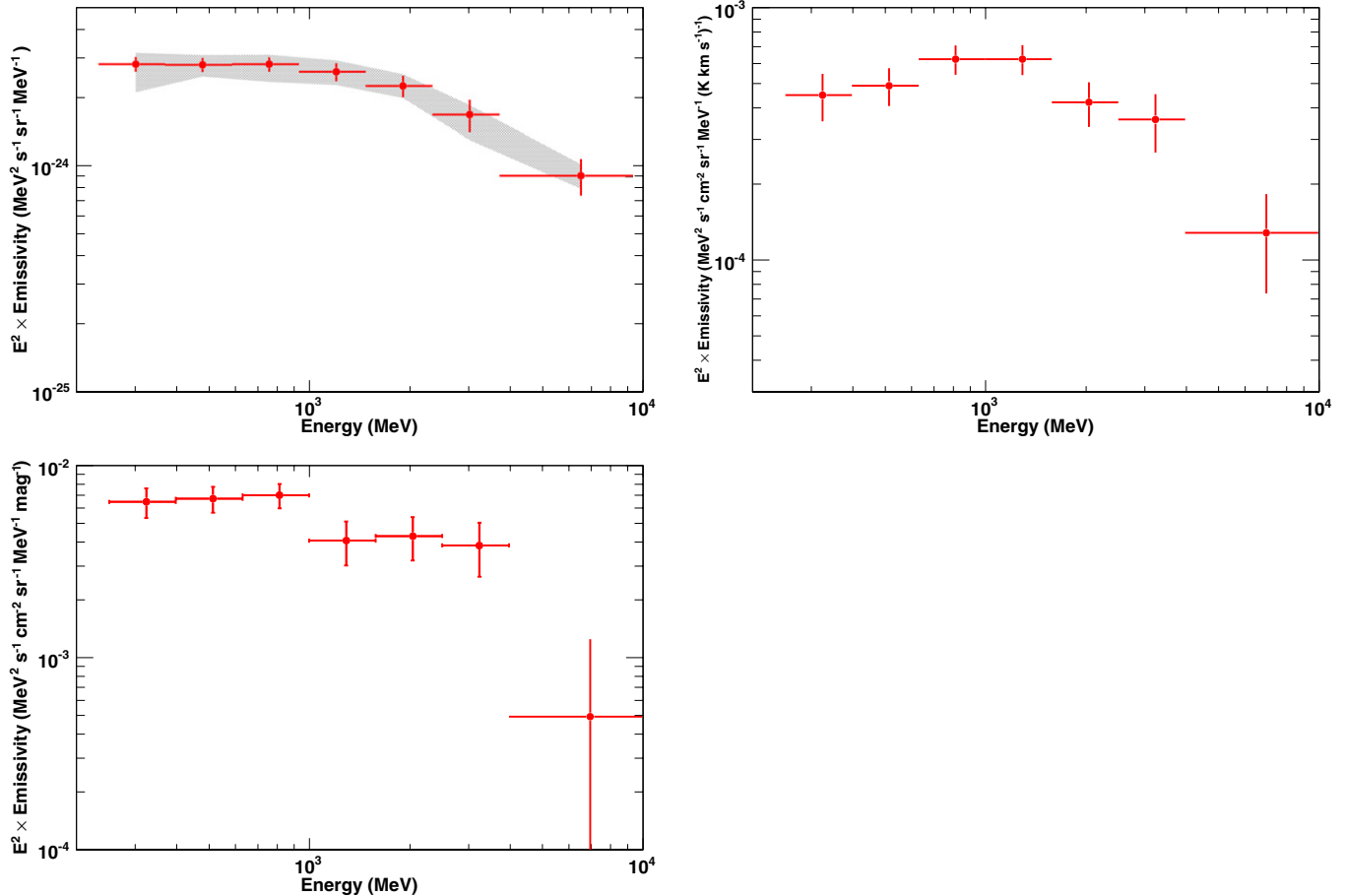
Figure 14. Same as Figure 13 for the R CrA region.
(A color version of this figure is available in the online journal.)

be significantly worse: the obtained $\ln(L)$ is lowered by 153 with eight less free parameters. In addition, the normalization of the IC term is lowered by more than a factor of three, although we cannot rule out such a low IC flux (low CR electron flux) for the direction of the Chamaeleon region. The effect of unresolved point sources is small, since we have verified that the obtained emissivities are robust against the lower threshold for point sources between TS = 50 and 100 (see Section 2.3). We also confirmed that the residual excess of photons around ($l = 280°$ to $288°$, $b = -20°$ to $-12°$; see the bottom panel of Figure 8) does not affect the local H I emissivity very much. Thus, the total systematic uncertainty of the Chamaeleon region is conservatively estimated to be $\sim$15% at most (mainly due to the T_S, isotropic component and IC models), indicating a difference of the CR density between the Chamaeleon and the others as shown in Figure 16.

If the CR density has a variation by a factor of 1.2–1.5 in the neighborhood of the solar system, then this requires a serious reconsideration of a smooth CR density often adopted for simplicity, and may have an impact on the study of the CR source distribution and diffuse γ-ray emission. We note that CR sources are stochastically distributed in space and time, and this may produce a CR anisotropy depending on the propagation conditions as discussed by, e.g., Blasi & Amato (2012a, 2012b). Study of other regions and more detailed theoretical calculations will be needed to further investigate this issue.

4.2. Molecular Masses in the Interstellar Clouds Studied

Since the γ-ray production is almost independent of the chemical or thermodynamical state of the interstellar gas, the γ-ray observation is a powerful probe to investigate the molecular mass calibration ratio, X_{CO}, defined as $N(H_2)/W_{CO}$. Under the hypothesis that the same CR flux penetrates the H I and CO phases of an interstellar complex, we can calculate X_{CO} as $X_{CO} = q_{CO}/(2q_{HI})$, as shown in Figure 17 (left). The linear relation supports the assumption that Galactic CRs penetrate these molecular clouds uniformly to their cores. This also indicates that any contamination from point sources and CR spectral variations in molecular clouds analyzed here is small.

We have obtained X_{CO} by fitting the relation between q_{HI} and q_{CO} with a linear function using a maximum likelihood method; the X_{CO} values are $(0.96 \pm 0.06_{stat}\ {}^{+0.15}_{-0.12}{}_{sys}) \times 10^{20}$ cm^{-2} (K km s^{-1})$^{-1}$, $(0.99 \pm 0.08_{stat}\ {}^{+0.18}_{-0.10}{}_{sys}) \times 10^{20}$ cm^{-2} (K km s^{-1})$^{-1}$, and $(0.63 \pm 0.02_{stat}\ {}^{+0.09}_{-0.07}{}_{sys}) \times 10^{20}$ cm^{-2} (K km s^{-1})$^{-1}$ for the Chamaeleon, R CrA, and Cepheus and Polaris flare regions, respectively. The obtained value of X_{CO} for the Cepheus and Polaris flare region is $\sim$20% lower than that reported by Abdo et al. (2010b). Abdo et al. (2010b) also include in their study the Cassiopeia molecular cloud in the Gould Belt, and due to different ROIs considered, the q_{HI} emissivity was also different. X_{CO} of the Chamaeleon region is similar to that of the R CrA region, whereas that of the Cepheus and Polaris
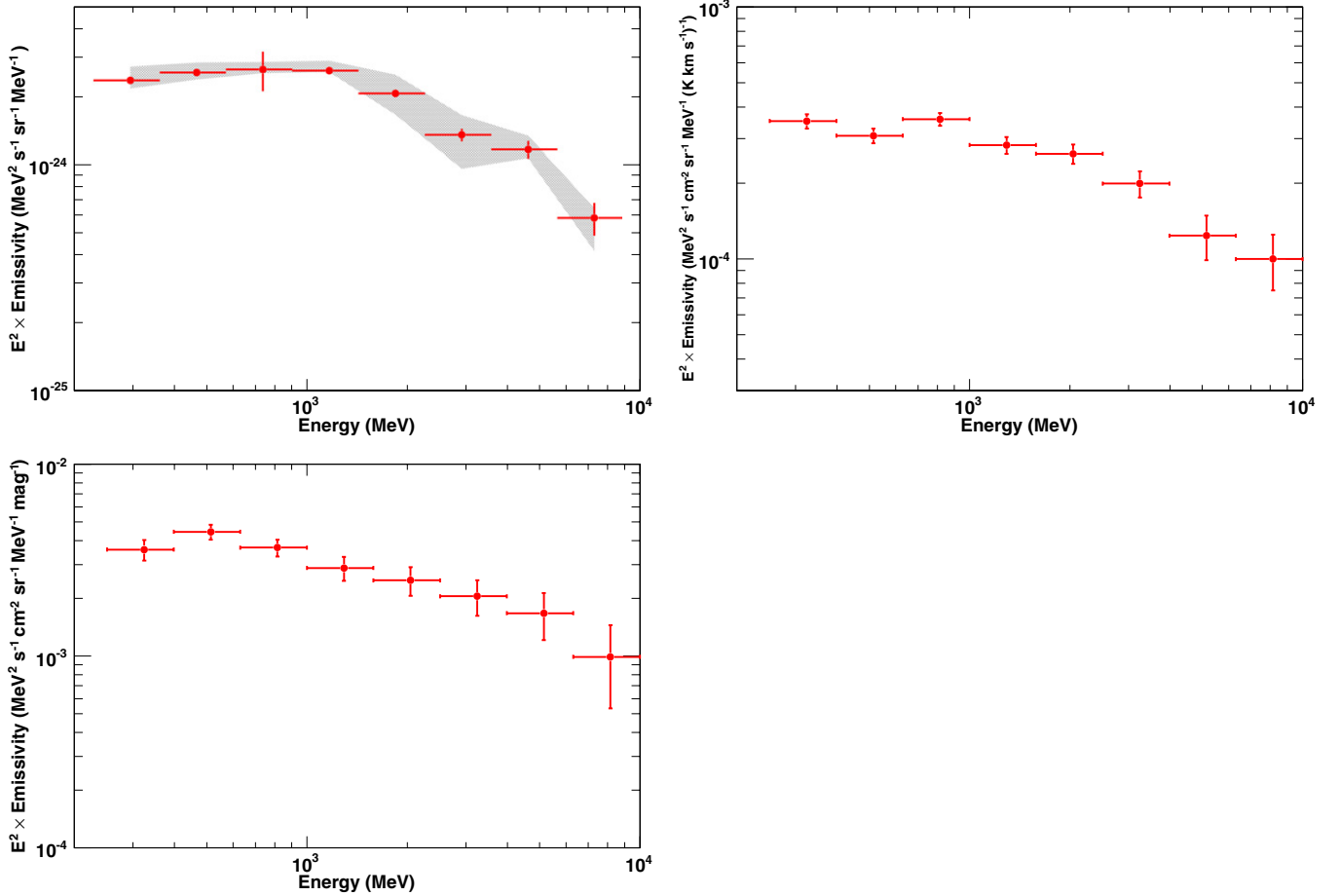
Figure 15. Same as Figure 13 for the Cepheus and Polaris flare region.

(A color version of this figure is available in the online journal.)
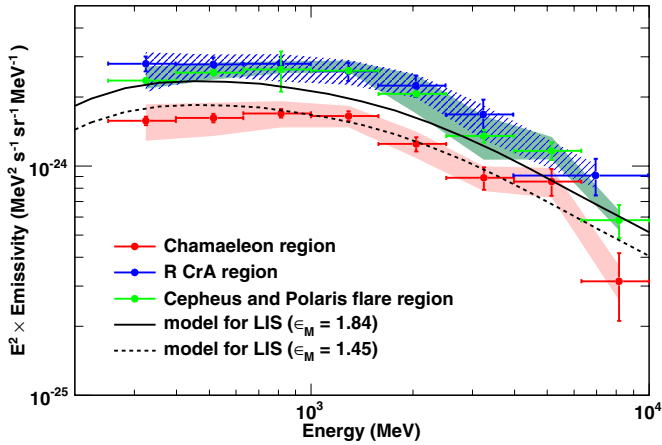

Figure 16. H I emissivity spectra of the Chamaeleon, R CrA, and Cepheus and Polaris flare regions compared with the model for the LIS with nuclear enhancement factors of 1.45 and 1.84. The shaded areas for the Chamaeleon, R CrA, and Cepheus and Polaris flare spectra indicate the systematic uncertainty evaluated in Section 3.

(A color version of this figure is available in the online journal.)

flare region is ∼2/3 of the others. The LAT data thus suggest a variation of X_{CO} on a ∼300 pc scale.

We can estimate the CO-bright molecular mass for the Chamaeleon, R CrA, and Cepheus and Polaris flare regions.

The mass of the gas traced by W_{CO} is expressed as

$$\frac{M}{M_\odot} = 2\mu \frac{m_H}{M_\odot} d^2 X_{CO} \int W_{CO}(l, b)\, d\Omega, \qquad (2)$$

where d is the distance to the cloud, m_H is the mass of the hydrogen atom and $\mu = 1.36$ is the mean atomic weight per H-atom (Allen 1973). From this equation, the mass of gas traced by CO is expressed as M_{CO} in Table 4: we obtained ∼5 × $10^3\, M_\odot$, ∼$10^3\, M_\odot$, and ∼3.3 × $10^4\, M_\odot$ for the Chamaeleon, R CrA, and Cepheus and Polaris flare regions, respectively. The obtained mass of the Cepheus and Polaris flare region is ∼20% lower than that reported by Abdo et al. (2010b) due to the different value of X_{CO}. Our estimates for the Chamaeleon and the R CrA regions are ∼1/2 of those by Dame et al. (1987); they obtained ∼$10^4\, M_\odot$ and ∼3 × $10^3\, M_\odot$ for the Chamaeleon and R CrA regions, respectively, under the assumption of a high value of $X_{CO} = 2.7 \times 10^{20}$ cm^{-2} (K km s^{-1})$^{-1}$.

Using the relation between $q_{H I}$ and q_{Av}, we can also calculate the mass of additional interstellar gas traced by Av_{res}. Figure 17 shows the results of the fitting by a linear relation, $q_{Av} = X_{Av} \cdot q_{H I}$. The obtained X_{Av} values are $(0.22 \pm 0.01_{stat} \pm 0.08_{sys}) \times 10^{22}$ cm^{-2} mag^{-1}, $(0.21 \pm 0.01_{stat} \pm 0.02_{sys}) \times 10^{22}$ cm^{-2} mag^{-1}, and $(0.14 \pm 0.01_{stat} \pm 0.03_{sys}) \times 10^{22}$ cm^{-2} mag^{-1} for the Chamaeleon, the R CrA, and Cepheus and Polaris flare regions, respectively. With a procedure similar to that for CO, we can calculate the mass of additional gas traced by Av_{res} expressed as $M_{Av_{res}}$ in Table 4: we obtained ∼2.0 × $10^4\, M_\odot$, ∼$10^3\, M_\odot$, and
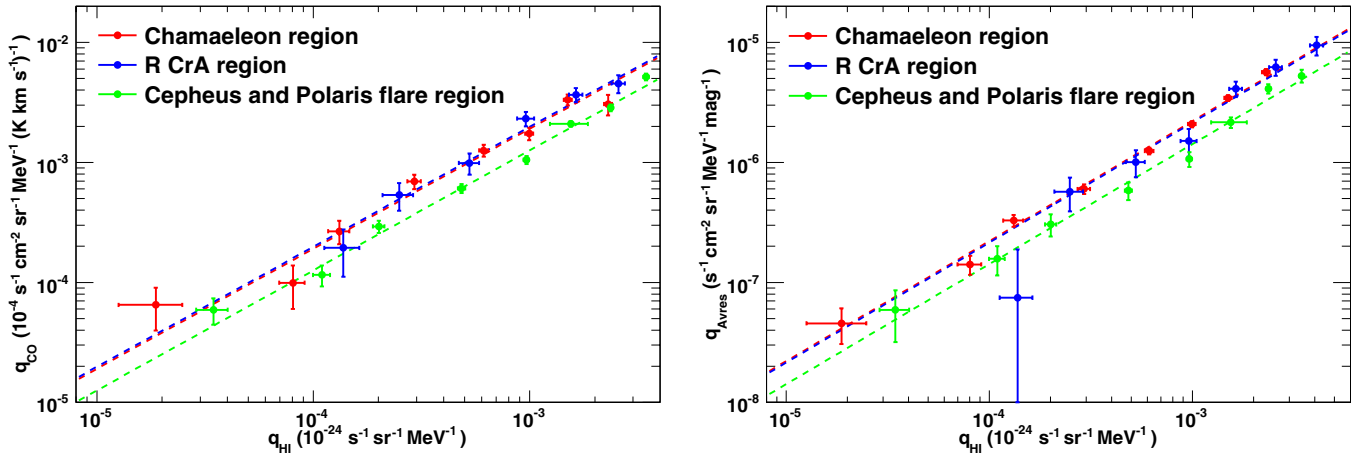
Figure 17. CO (left) and Av_{res} (right) vs. H I emissivities. Each point corresponds to an energy bin (see Tables 1–3). Errors are statistical only.
(A color version of this figure is available in the online journal.)

Table 4
Masses in the Interstellar Clouds for Each Region

Region	l	b	d (pc)	M_{CO} ($M_\odot$)	$M_{Av_{res}}$ ($M_\odot$)
Chamaeleon	$[295°, 305°]$	$[-20°, -12°]$	215^a	$\sim 5 \times 10^3$	$\sim 2.0 \times 10^4$
R CrA	$[-1°, 4°]$	$[-24°, -16°]$	150^a	$\sim 10^3$	$\sim 10^3$
Cepheus and Polaris flare	$[100°, 125°]$	$[15°, 30°]$	300^b	$\sim 3.3 \times 10^4$	$\sim 1.3 \times 10^4$

Notes.
[a] Dame et al. (1987).
[b] Abdo et al. (2010b).

$\sim 1.3 \times 10^4 \, M_\odot$ for the Chamaeleon, R CrA, and Cepheus and Polaris flare regions, respectively. We thus obtained mass estimates for the Chamaeleon and R CrA regions similar to previous ones (Dame et al. 1987) if we consider the total mass (traced by W_{CO} and Av_{res}), although the procedure is not straightforward since the gas traced by Av_{res} is extended in a much larger region of the sky. Detailed study of the matter distribution in the interstellar space by comparing γ-rays and other tracers will be reported elsewhere.

5. SUMMARY AND CONCLUSIONS

We have studied the γ-ray emission from the Chamaeleon, R CrA, and Cepheus and Polaris flare molecular clouds close to the solar system ($\lesssim 300$ pc) using the first 21 months of *Fermi* LAT data. Thanks to the excellent performance of the LAT, we have obtained unprecedentedly high-quality emissivity spectra of the atomic and molecular gas in these regions in the 250 MeV–10 GeV range.

The γ-ray emissivity spectral shapes in three regions agree well with the model for the LIS (a model based on local CR measurement), thus indicating a similar spectral distribution of CRs in these regions. The emissivities, however, indicate a variation of the CR density of $\sim 20\%$ within ~ 300 pc around the solar system, even if we consider the systematic uncertainties. We consider possible origins of the variation are non-uniform supernova rate and anisotropy of CRs depending on the propagation conditions.

The molecular mass calibration ratio X_{CO} for the Chamaeleon cloud and the R CrA cloud are comparable, whereas that of the Cepheus and Polaris flare region is $\sim 2/3$ of the others, suggesting a variation of X_{CO} in the vicinity of the solar system.

From the obtained values of X_{CO}, the masses of gas traced by W_{CO} in the Chamaeleon, R CrA, and Cepheus and Polaris flare regions are estimated to be $\sim 5 \times 10^3 \, M_\odot$, $\sim 10^3 \, M_\odot$, and $\sim 3.3 \times 10^4 \, M_\odot$, respectively. Similar amounts of gas are inferred to be in the phase not well traced by the H I or CO lines. Accumulation of more γ-ray data, particularly at high energies, and progress in ISM studies, will reveal the CR and matter distribution in greater detail.

REFERENCES

Abdo, A. A., Ackermann, M., Ajello, M., et al. 2009a, Astropart. Phys., 32, 193
Abdo, A. A., Ackermann, M., Ajello, M., et al. 2009b, Phys. Rev. Lett., 103, 251101
Abdo, A. A., Ackermann, M., Ajello, M., et al. 2009c, ApJ, 703, 1249
Abdo, A. A., Ackermann, M., Ajello, M., et al. 2010a, ApJS, 188, 405
Abdo, A. A., Ackermann, M., Ajello, M., et al. 2010b, ApJ, 710, 133
Ackermann, M., Ajello, M., Atwood, W. B., et al. 2012, ApJ, 750, 3
Ackermann, M., Ajello, M., Baldini, L., et al. 2011, ApJ, 726, 81
Alcaraz, J., Alvisi, D., Alpat, B., et al. 2000, Phys. Lett. B, 472, 215
Allen, C. W. 1973, Astrophysical Quantities (London: Athlone)
Atwood, W. B., Abdo, A. A., Ackermann, M., et al. 2009, ApJ, 697, 1071
Blasi, P., & Amato, E. 2012a, J. Cosmol. Astropart. Phys., JCAP01(2012a)010
Blasi, P., & Amato, E. 2012b, J. Cosmol. Astropart. Phys., JCAP01(2012b)011
Bloemen, J. B. G. M., Caraveo, P. A., Hermsen, W., et al. 1984, A&A, 139, 37
Case, G. L., & Bhattacharya, D. 1998, ApJ, 504, 761
Clemens, D. P. 1985, ApJ, 295, 422
Dame, T. M. 2011, arXiv:1101.1499
Dame, T. M., Hartmann, D., & Thaddeus, P. 2001, ApJ, 547, 792
Dame, T. M., Ungerechts, H., Cohen, R. S., et al. 1987, ApJ, 322, 706
Digel, S. W., Aprile, E., Hunter, S. D., Mukherjee, R., & Xu, F. 1999, ApJ, 520, 196
Grenier, I. A., Casandjian, J. M., & Terrier, R. 2005, Science, 307, 1292
Hunter, S. D., Digel, S. W., de Geus, E. J., & Kanbach, G. 1994, ApJ, 436, 216
Kalberla, P. M. W., Burton, W. B., Hartmann, D., et al. 2005, A&A, 440, 775
Lebrun, F., Bennett, K., Bignami, G. F., et al. 1983, ApJ, 274, 231
Lorimer, D. R. 2004, in IAU Symp. 218, Young Neutron Stars and Their Environments, ed. F. Camilo & B. M. Gaensler (San Francisco, CA: ASP), 105
Mattox, J. R., Bertsch, D. L., Chiang, J., et al. 1996, ApJ, 461, 396
Mori, M. 2009, Astropart. Phys., 31, 341
Perrot, C. A., & Grenier, I. A. 2003, A&A, 404, 519
Porter, T. A., Moskalenko, I. V., Strong, A. W., Orlando, E., & Bouchet, L. 2008, ApJ, 682, 400
Rando, R., & the Fermi LAT Collaboration 2009, arXiv:0907.0626
Sanuki, T., Motoki, M., Matsumoto, H., et al. 2000, ApJ, 545, 1135
Schlegel, D. J., Finkbeiner, D. P., & Daris, M. 1998, ApJ, 500, 525
Strong, A. W., & Moskalenko, I. V. 1998, ApJ, 509, 212
Su, M., Slatyer, T. R., & Finkbeiner, D. P. 2010, ApJ, 724, 1044

ERRATUM: "FERMI LARGE AREA TELESCOPE STUDY OF COSMIC-RAYS AND THE INTERSTELLAR MEDIUM IN NEARBY MOLECULAR CLOUDS" (2012, ApJ, 755, 22)

M. ACKERMANN[1], M. AJELLO[2], A. ALLAFORT[2], L. BALDINI[3], J. BALLET[4], G. BARBIELLINI[5,6], D. BASTIERI[7,8], K. BECHTOL[2], R. BELLAZZINI[3], B. BERENJI[2], R. D. BLANDFORD[2], E. D. BLOOM[2], E. BONAMENTE[9,10], A. W. BORGLAND[2], E. BOTTACINI[2], T. J. BRANDT[11,12], J. BREGEON[3], M. BRIGIDA[13,14], P. BRUEL[15], R. BUEHLER[2], G. BUSETTO[7,8], S. BUSON[7,8], G. A. CALIANDRO[16], R. A. CAMERON[2], P. A. CARAVEO[17], J. M. CASANDJIAN[4], C. CECCHI[9,10], E. CHARLES[2], A. CHEKHTMAN[18,63], J. CHIANG[2], S. CIPRINI[10,19], R. CLAUS[2], J. COHEN-TANUGI[20], J. CONRAD[21,22,64], F. D'AMMANDO[9,23,24], A. DE ANGELIS[25], F. DE PALMA[13,14], C. D. DERMER[26], S. W. DIGEL[2], E. DO COUTO E SILVA[2], P. S. DRELL[2], A. DRLICA-WAGNER[2], L. FALLETTI[20], C. FAVUZZI[13,14], S. J. FEGAN[15], E. C. FERRARA[27], W. B. FOCKE[2], Y. FUKAZAWA[28], Y. FUKUI[29], S. FUNK[2], P. FUSCO[13,14], F. GARGANO[14], D. GASPARRINI[30], S. GERMANI[9,10], N. GIGLIETTO[13,14], F. GIORDANO[13,14], M. GIROLETTI[31], T. GLANZMAN[2], G. GODFREY[2], I. A. GRENIER[4], M.-H. GRONDIN[32,33], J. E. GROVE[26], S. GUIRIEC[34], D. HADASCH[16], Y. HANABATA[28], A. K. HARDING[27], K. HAYASHI[35], D. HORAN[15], X. HOU[36], R. E. HUGHES[37], R. ITOH[28], M. S. JACKSON[22,38], G. JÓHANNESSON[39], A. S. JOHNSON[2], T. KAMAE[2], H. KATAGIRI[40], J. KATAOKA[41], J. KNÖDLSEDER[11,12], M. KUSS[3], J. LANDE[2], S. LARSSON[21,22,42], S.-H. LEE[43], M. LEMOINE-GOUMARD[44,65], F. LONGO[5,6], F. LOPARCO[13,14], M. N. LOVELLETTE[26], P. LUBRANO[9,10], P. MARTIN[45], M. N. MAZZIOTTA[14], J. E. MCENERY[27,46], J. MEHAULT[20], P. F. MICHELSON[2], W. MITTHUMSIRI[2], T. MIZUNO[28], A. A. MOISEEV[46,47], C. MONTE[13,14], M. E. MONZANI[2], A. MORSELLI[48], I. V. MOSKALENKO[2], S. MURGIA[2], M. NAUMANN-GODO[4], R. NEMMEN[27], S. NISHINO[28], J. P. NORRIS[49], E. NUSS[20], M. OHNO[35], T. OHSUGI[50], A. OKUMURA[2,35], N. OMODEI[2], E. ORLANDO[2], J. F. ORMES[51], M. OZAKI[35], D. PANEQUE[2,52], J. H. PANETTA[2], D. PARENT[18,63], M. PESCE-ROLLINS[3], M. PIERBATTISTA[4], F. PIRON[20], G. PIVATO[8], T. A. PORTER[2], S. RAINÒ[13,14], R. RANDO[7,8], M. RAZZANO[3,53], A. REIMER[2,54], O. REIMER[2,54], C. ROMOLI[8], M. ROTH[55], T. SADA[28], H. F.-W. SADROZINSKI[53], D. A. SANCHEZ[32], C. SBARRA[7], C. SGRÒ[3], E. J. SISKIND[56], G. SPANDRE[3], P. SPINELLI[13,14], A. W. STRONG[45], D. J. SUSON[57], H. TAKAHASHI[50], T. TAKAHASHI[35], T. TANAKA[2], J. G. THAYER[2], J. B. THAYER[2], D. J. THOMPSON[27], L. TIBALDO[7,8], O. TIBOLLA[58], M. TINIVELLA[3], D. F. TORRES[16,59], G. TOSTI[9,10], A. TRAMACERE[2,60,61], E. TROJA[27,66], Y. UCHIYAMA[2], T. UEHARA[28], T. L. USHER[2], J. VANDENBROUCKE[2], V. VASILEIOU[20], G. VIANELLO[2,60], V. VITALE[48,62], A. P. WAITE[2], P. WANG[2], B. L. WINER[37], K. S. WOOD[26], H. YAMAMOTO[29], Z. YANG[21,22], AND S. ZIMMER[21,22]

[1] Deutsches Elektronen Synchrotron DESY, D-15738 Zeuthen, Germany
[2] W. W. Hansen Experimental Physics Laboratory, Kavli Institute for Particle Astrophysics and Cosmology, Department of Physics and SLAC National Accelerator Laboratory, Stanford University, Stanford, CA 94305, USA
[3] Istituto Nazionale di Fisica Nucleare, Sezione di Pisa, I-56127 Pisa, Italy
[4] Laboratoire AIM, CEA-IRFU/CNRS/Université Paris Diderot, Service d'Astrophysique, CEA Saclay, 91191 Gif sur Yvette, France
[5] Istituto Nazionale di Fisica Nucleare, Sezione di Trieste, I-34127 Trieste, Italy
[6] Dipartimento di Fisica, Università di Trieste, I-34127 Trieste, Italy
[7] Istituto Nazionale di Fisica Nucleare, Sezione di Padova, I-35131 Padova, Italy
[8] Dipartimento di Fisica "G. Galilei," Università di Padova, I-35131 Padova, Italy
[9] Istituto Nazionale di Fisica Nucleare, Sezione di Perugia, I-06123 Perugia, Italy
[10] Dipartimento di Fisica, Università degli Studi di Perugia, I-06123 Perugia, Italy
[11] CNRS, IRAP, F-31028 Toulouse cedex 4, France
[12] GAHEC, Université de Toulouse, UPS-OMP, IRAP, Toulouse, France
[13] Dipartimento di Fisica "M. Merlin" dell'Università e del Politecnico di Bari, I-70126 Bari, Italy
[14] Istituto Nazionale di Fisica Nucleare, Sezione di Bari, 70126 Bari, Italy
[15] Laboratoire Leprince-Ringuet, École polytechnique, CNRS/IN2P3, Palaiseau, France
[16] Institut de Ciències de l'Espai (IEEE-CSIC), Campus UAB, 08193 Barcelona, Spain
[17] INAF-Istituto di Astrofisica Spaziale e Fisica Cosmica, I-20133 Milano, Italy
[18] Center for Earth Observing and Space Research, College of Science, George Mason University, Fairfax, VA 22030, USA
[19] ASI Science Data Center, I-00044 Frascati (Roma), Italy
[20] Laboratoire Univers et Particules de Montpellier, Université Montpellier 2, CNRS/IN2P3, Montpellier, France
[21] Department of Physics, Stockholm University, AlbaNova, SE-106 91 Stockholm, Sweden
[22] The Oskar Klein Centre for Cosmoparticle Physics, AlbaNova, SE-106 91 Stockholm, Sweden
[23] IASF Palermo, 90146 Palermo, Italy
[24] INAF-Istituto di Astrofisica Spaziale e Fisica Cosmica, I-00133 Roma, Italy
[25] Dipartimento di Fisica, Università di Udine and Istituto Nazionale di Fisica Nucleare, Sezione di Trieste, Gruppo Collegato di Udine, I-33100 Udine, Italy
[26] Space Science Division, Naval Research Laboratory, Washington, DC 20375-5352, USA
[27] NASA Goddard Space Flight Center, Greenbelt, MD 20771, USA
[28] Department of Physical Sciences, Hiroshima University, Higashi-Hiroshima, Hiroshima 739-8526, Japan; mizuno@hirax6.hepl.hiroshima-u.ac.jp
[29] Department of Physics and Astrophysics, Nagoya University, Chikusa-ku Nagoya 464-8602, Japan
[30] Agenzia Spaziale Italiana (ASI) Science Data Center, I-00044 Frascati (Roma), Italy
[31] INAF Istituto di Radioastronomia, 40129 Bologna, Italy
[32] Max-Planck-Institut für Kernphysik, D-69029 Heidelberg, Germany
[33] Landessternwarte, Universität Heidelberg, Königstuhl, D 69117 Heidelberg, Germany
[34] Center for Space Plasma and Aeronomic Research (CSPAR), University of Alabama in Huntsville, Huntsville, AL 35899, USA
[35] Institute of Space and Astronautical Science, JAXA, 3-1-1 Yoshinodai, Chuo-ku, Sagamihara, Kanagawa 252-5210, Japan; khayashi@astro.isas.jaxa.jp
[36] Centre d'Études Nucléaires de Bordeaux Gradignan, IN2P3/CNRS, Université Bordeaux 1, BP120, F-33175 Gradignan Cedex, France
[37] Department of Physics, Center for Cosmology and Astro-Particle Physics, The Ohio State University, Columbus, OH 43210, USA
[38] Department of Physics, Royal Institute of Technology (KTH), AlbaNova, SE-106 91 Stockholm, Sweden
[39] Science Institute, University of Iceland, IS-107 Reykjavik, Iceland
[40] College of Science, Ibaraki University, 2-1-1, Bunkyo, Mito 310-8512, Japan

1

[41] Research Institute for Science and Engineering, Waseda University, 3-4-1, Okubo, Shinjuku, Tokyo 169-8555, Japan
[42] Department of Astronomy, Stockholm University, SE-106 91 Stockholm, Sweden
[43] Yukawa Institute for Theoretical Physics, Kyoto University, Kitashirakawa Oiwake-cho, Sakyo-ku, Kyoto 606-8502, Japan
[44] Université Bordeaux 1, CNRS/IN2p3, Centre d'Études Nucléaires de Bordeaux Gradignan, 33175 Gradignan, France
[45] Max-Planck Institut für extraterrestrische Physik, 85748 Garching, Germany
[46] Department of Physics and Department of Astronomy, University of Maryland, College Park, MD 20742, USA
[47] Center for Research and Exploration in Space Science and Technology (CRESST) and NASA Goddard Space Flight Center, Greenbelt, MD 20771, USA
[48] Istituto Nazionale di Fisica Nucleare, Sezione di Roma "Tor Vergata," I-00133 Roma, Italy
[49] Department of Physics, Boise State University, Boise, ID 83725, USA
[50] Hiroshima Astrophysical Science Center, Hiroshima University, Higashi-Hiroshima, Hiroshima 739-8526, Japan
[51] Department of Physics and Astronomy, University of Denver, Denver, CO 80208, USA
[52] Max-Planck-Institut für Physik, D-80805 München, Germany
[53] Santa Cruz Institute for Particle Physics, Department of Physics and Department of Astronomy and Astrophysics,
University of California at Santa Cruz, Santa Cruz, CA 95064, USA
[54] Institut für Astro- und Teilchenphysik and Institut für Theoretische Physik, Leopold-Franzens-Universität Innsbruck, A-6020 Innsbruck, Austria
[55] Department of Physics, University of Washington, Seattle, WA 98195-1560, USA
[56] NYCB Real-Time Computing Inc., Lattingtown, NY 11560-1025, USA
[57] Department of Chemistry and Physics, Purdue University Calumet, Hammond, IN 46323-2094, USA
[58] Institut für Theoretische Physik and Astrophysik, Universität Würzburg, D-97074 Würzburg, Germany
[59] Institució Catalana de Recerca i Estudis Avançats (ICREA), Barcelona, Spain
[60] Consorzio Interuniversitario per la Fisica Spaziale (CIFS), I-10133 Torino, Italy
[61] INTEGRAL Science Data Centre, CH-1290 Versoix, Switzerland
[62] Dipartimento di Fisica, Università di Roma "Tor Vergata," I-00133 Roma, Italy

Online-only material: color figures

In the published version of the paper, errors were made in calculating the exposure time due to an analysis mistake. While they do not affect gas emissivities of the R CrA and Cepheus & Polaris flare regions significantly (the differences are within the systematic uncertainty), that of the Chamaeleon region is increased by ∼20%. Although we claimed a difference of ∼50% in gas emissivity among these molecular cloud regions in the original paper, it is decreased to ∼30% (comparable to the sum of the statistical and systematic uncertainties) in the revised analysis. Therefore, our conclusion of the original paper, that a small variation (∼20%) of the CR density in the solar neighborhood exists, is not supported by the data if we take these uncertainties into account. On the other hand, the obtained X_{CO} and X_{Av} values, and the masses of gas calculated from them are not changed significantly (the differences are within the statistical errors). Errors and corrections in the original paper are summarized below.

1. In the Abstract (lines 5–6) and Section 3 (lines 4–5 in the 3rd paragraph) in the original paper, the γ-ray emissivity above 250 MeV for the Chamaeleon region should be $(7.2 \pm 0.1_{stat} \pm 1.0_{sys}) \times 10^{-27}$ photons s^{-1} sr^{-1} H-atom^{-1}, not $(5.9 \pm 0.1_{stat}\ ^{+0.9}_{-1.0sys}) \times 10^{-27}$ photons s^{-1} sr^{-1} H-atom^{-1}.

2. In the Abstract (lines 8–10), "Whereas the energy dependences of the emissivities agree well with that predicted from direct CR observations at the Earth, the measured emissivities from 250 MeV to 10 GeV indicate a variation of the CR density by ∼20% in the neighborhood of the solar system, even if we consider the systematic uncertainties." should be changed to "The energy dependences of the emissivities agree well with that predicted from direct CR observations at the Earth. Although the measured emissivities from 250 MeV to 10 GeV differ by ∼30% among these molecular cloud regions, the difference is not significant if we take the systematic uncertainty into account."

3. Table 1 and Figure 13, which show gas emissivities and spectra for the Chamaeleon region in the original paper, should be changed to the Table 1 and Figure 1 as shown below.

4. Figure 16, which compares H i gas emissivities among several regions in the original paper, should be changed to Figure 2 as shown below.

5. The text from the line 13 to the last one in the first paragraph of Section 4.1, "The spectral shapes for the three regions..., indicating a difference of the CR density between the Chamaeleon and the others as shown in Figure 16." should be changed to the paragraph that follows.

"The shaded area of each spectrum indicates the systematic uncertainty as described in Section 3. We note that the systematic uncertainty of the LAT effective area (5% at 100 MeV and 20% at 10 GeV; Rando et al. 2009) does not affect the relative value of emissivities. The effect of unresolved point sources is small; we have verified that the obtained emissivities are almost unaffected by decreasing the threshold for point sources from TS = 100 to TS = 50. We also confirmed that the residual excess of photons around ($l = 280°$ to $288°$, $b = -20°$ to $-12°$; see the bottom panel of Figure 8) in the Chamaeleon region does not affect the local H i emissivity very much. Thus the total systematic uncertainty is reasonably expressed by the shaded area shown in
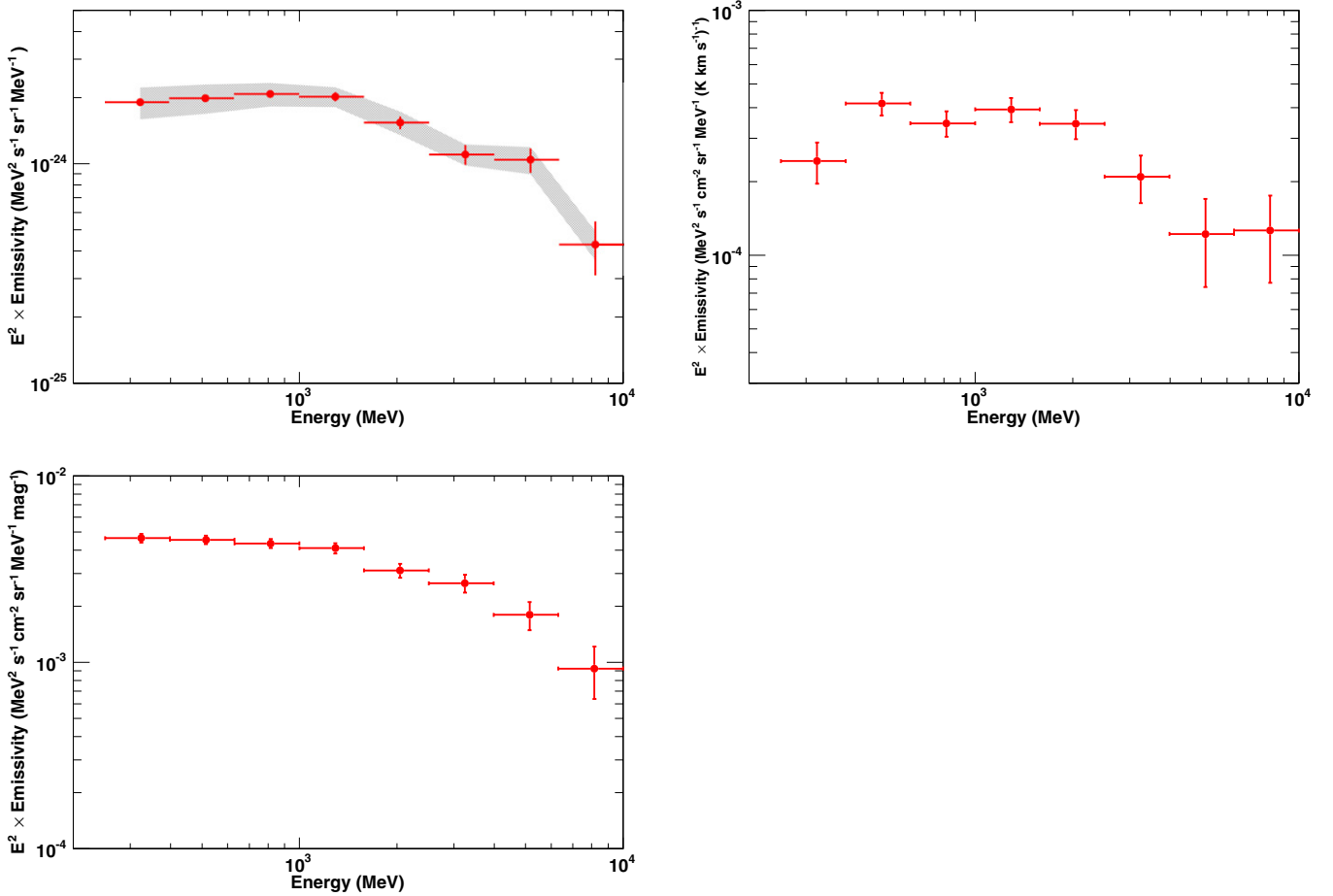
Figure 1. Emissivity spectrum of the local H I gas (top left), that per W_{CO} unit (top right), and that per unit $A_{v_{res}}$ magnitude (bottom left) of the Chamaeleon region. The shaded area shows systematic uncertainties for H I (see the text for details).

(A color version of this figure is available in the online journal.)

Table 1
Gas Emissivities in the Chamaeleon Region with Their Statistical Uncertainties
(Assuming $T_S = 125$ K for the H I Maps Preparation)

Energy (GeV)	$q_{H I,1}$	q_{CO}	q_{Av}
0.25–0.40	2.8 ± 0.1	0.35 ± 0.07	0.68 ± 0.04
0.40–0.63	1.83 ± 0.07	0.39 ± 0.04	0.42 ± 0.02
0.63–1.00	1.21 ± 0.05	0.20 ± 0.02	0.25 ± 0.01
1.00–1.58	0.74 ± 0.03	0.15 ± 0.02	0.15 ± 0.01
1.58–2.51	0.36 ± 0.02	0.08 ± 0.01	0.073 ± 0.006
2.51–3.98	0.16 ± 0.02	0.031 ± 0.006	0.039 ± 0.004
3.98–6.31	0.10 ± 0.01	0.011 ± 0.004	0.017 ± 0.003
6.31–10.00	0.025 ± 0.007	0.008 ± 0.003	0.006 ± 0.002
Total	7.2 ± 0.1	1.22 ± 0.09	1.64 ± 0.05

Notes. Units; $q_{H I,1}$ (10^{-27} s^{-1} sr^{-1}), q_{CO} (10^{-6} cm^{-2} s^{-1} sr^{-1} (K km s^{-1})$^{-1}$), q_{Av} (10^{-5} cm^{-2} s^{-1} sr^{-1} mag^{-1}).

Figure 2. The spectral shapes for the three regions agree well with the LIS models, indicating that the CR nuclei have similar spectral distribution in the vicinity of the solar system. On the other hand, the apparent difference of emissivities among the three regions (by $\sim$30%) is comparable to the uncertainty (statistical and systematic errors). Therefore the LAT data do not allow us to claim or exclude a possible small variation of the CR density in the solar neighborhood."

6. In Section 5 (lines 4–9 in the 2nd paragraph), "The emissivities, however, indicate a variation of the CR density by $\sim$20% within $\sim$300 pc around the solar system, even if we consider the systematic uncertainties. We consider possible origins of the variation are non-uniform supernova rate and anisotropy of CRs depending on the propagation conditions" should be changed to "Although the emissivities differ by $\sim$30% among these regions, the difference is not significant if we take the systematic uncertainty into account. If the variation really exists, possible origins of it might be non-uniform supernova rate and anisotropy of CRs, depending on the propagation conditions."
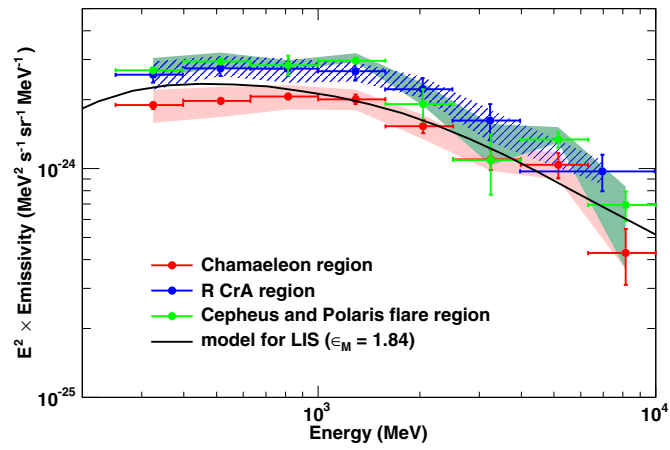
Figure 2. H I emissivity spectra of the Chamaeleon, R CrA, and Cepheus & Polaris flare regions compared with the model for the LIS with the nuclear enhancement factor of 1.84. The shaded areas for the Chamaeleon, R CrA, and Cepheus and Polaris flare spectra indicate the systematic uncertainty evaluated in Section 3.

(A color version of this figure is available in the online journal.)

REFERENCE

Rando, R., & the Fermi LAT Collaboration 2009, arXiv:0907.0626